ABSTRACT

Title of thesis: LABORATORY STUDIES ON THE GENERATION OF FIREBRANDS FROM CYLINDRICAL WOODEN DOWELS

Sara Caton, Master of Science, 2016

Thesis directed by: Professor Michael J. Gollner
Department of Fire Protection Engineering

Wildland urban interface (WUI) fires are increasing in size and severity in the United States. These fires are a major concern because they spread into communities and ignite thousands of homes every year. The main source of home ignitions is not through direct flame contact or radiation; rather, firebrands are the primary pathway for fire to spread into WUI communities. Firebrands are pieces of a burning material that break off and then can be lofted and carried large distances to ignite subsequent fires. The purpose of this thesis is to study the breakage process to better understand how firebrands are produced.

Cylindrical wooden dowels are used to represent vegetative fuels in WUI fires. The dowels were exposed to various heating conditions and then three-point bending tests were performed on each dowel to study the effect of combustion on strength properties. It has been found that there are two distinct regimes that describe the breakage. The size of the dowel and the final density of the dowel both control the transition between regimes. A scaling analysis was performed to show that

the two regimes and transition point are the same for all species. Predictions of wind velocities needed to produce the measured critical stresses were calculated, because a connection needs to be drawn between the combustion and the wind to fully understand firebrand generation.

LABORATORY STUDIES ON THE GENERATION OF FIREBRANDS FROM CYLINDRICAL WOODEN DOWELS

by

Sara Caton

Thesis submitted to the Faculty of the Graduate School of the
University of Maryland, College Park in partial fulfillment
of the requirements for the degree of
Master of Science
2016

Advisory Committee:
Professor Michael J. Gollner, Ph.D., Committee Chair
Professor James Milke, Ph.D.
Mr. Nelson Bryner, M.S.

Acknowledgments

I am grateful to Professor Michael Gollner for giving me the opportunity to work on the NFPA Research Foundation project on Pathways for Building Fire Spread at the Wildland Urban Interface (WUI) as an undergraduate. This project was my first exposure to the WUI fire problem and sparked my interest in the the topic. Learning of the large gaps of scientific knowledge that need to be filled to better understand the risks of WUI fires drove my passion to start filling in these gaps with this research.

I also need to thank Professor Michael Gollner for being my adviser for this research. His knowledge and devotion to fire science and wildfire science is inspiring. I will always be grateful for his immense support.

I am fortunate to have been funded as a Pathways Student in the Fire Research Division, WUI Group of the Engineering Laboratory at the National Institute of Standards and Technology (NIST). Many thanks to Nelson Bryner and Erica Kuligowski, both of whom provided me with continuous support and encouragement throughout this past year.

My colleagues in the Department of Fire Protection Engineering have helped to support me in many ways and made every day at work entertaining. Raquel Hakes, Paul Anderson, and Nate May were constant sources of advice and new perspectives in times of difficulties, and Matthew Weston-Dawkes was always ready to lend a helping hand, especially when it came to cutting dowels. All of the other members of the Gollner Lab Group and the FPE faculty and staff also played a very

meaningful part in getting me to this stage of my career.

I must thank my mom, dad, and sister, Theresa, for being exceptional roommates and keeping me sane, when things became overwhelming, and Nevin Kerr for always believing in me and reminding me not to take life too seriously. I will always be appreciative for the love and support of all my other close family members and friends. They are the best support system I could ask for.

Table of Contents

List of Tables

List of Figures

Chapter 1: Introduction

1.1 The Problem

The term wildland urban interface (WUI) describes a geographic location where humans and their communities meet or comingle with undeveloped wildland areas. A WUI community can be referred to as an interface community, where wildland fuels directly border development, or an intermix community, where wildland fuels are interspersed throughout development, and both of these types of communities are exposed to multiple risks from wildland fires. Although the concept of WUI fire risk is not new, it is a problem that is often overshadowed by the risk of structural fires. One reason for this is a difference in costs. Firefighting is the most apparent cost in wildfires, and although these costs have been increasing [1], the federal government typically incurs most of these costs. Structural fires, on the other hand, incur costs to homeowners and insurance companies, which are smaller on an incident-to-incident basis, but add up to significantly more [2]. WUI fires also receive less attention, because there are not as many human deaths associated with these fires when compared to structural fires. These factors result in a large gap of knowledge and, subsequently, multiple areas of research needs in WUI fire research.

Over the past few decades, fires in WUI communities have been increasing in

severity, resulting in large scale WUI disasters internationally every year [3]. Figure 1.1 shows that while the number of fires that have occurred in the United States over the past three decades is mostly steady, the size of the fires has been increasing and is expected to continue to increase due to extreme fire weather conditions and fuel buildups. In fact, current data shows that 97% of the area burned by wildfires in the United States is the result of only 3% of the fires occurring [1]. These trends are due to three main causes: climate change, fuel management policies, and in-

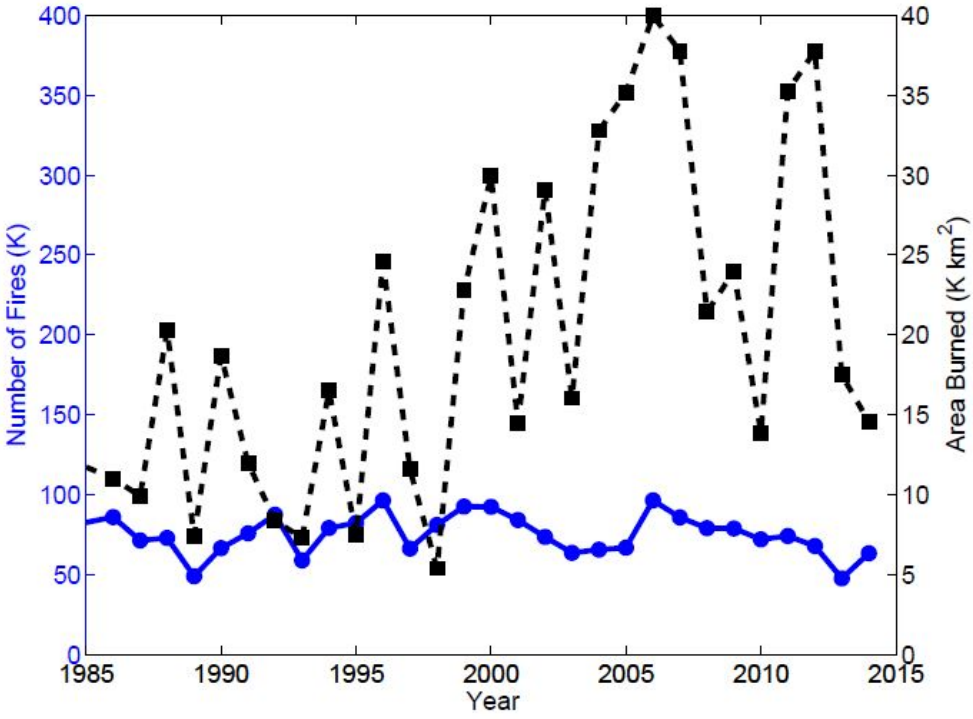

Figure 1.1: Although the number of fires (solid blue line) in the United States has remained generally steady over 30 years, the area burned (dashed black line) by fires has been increasing [1].

creased rural development. Climate change has contributed to drier environments, fuels with low moisture contents (MCs), and hotter temperatures, which all increase

wildfire potential and severity. Fire extinguishment of all wildland fires was a popular fuel management policy that actually made the wildland fire problem worse. Wildland vegetation has natural fire regimes that are a necessary part of fire ecology. Consequently, when wildland fires are extinguished, the natural fire regime of an area is altered and the vegetation becomes overgrown and untamed, adding to the fuel load of an area and intensifying burning conditions. Finally, development in traditionally rural areas is becoming a more popular trend. These developments are the WUI communities described above and introduce structures and humans to the WUI disaster sequence and ultimately create more ignition sources.

Because wildland fires are a natural part of fire ecology and without ignitable structures there would be no WUI disasters, the WUI fire problem can be thought of as a structure ignition problem [1,4]. There are three mechanisms for fire to spread to WUI communities and ignite homes: direct flame contact, radiation, and firebrands. It is rare for flames from the main fire front to come in direct contact with structures. Rather, flames from smaller fires (often caused by firebrands) will ignite adjacent structures or components, such as sheds, fences, or woodpiles, which will then spread to the home and expose it to direct flame contact. If vegetation is cleared and there is no combustible material surrounding or leading up to a home, the risk of direct flame contact exposure to a home can be decreased. Radiation, the second exposure condition, will occur when large flames are nearby and can subject a structure to radiant heating. Radiant exposure can be reduced or eliminated by keeping safe distances between structures and wildland fuels and adjacent structures. The last mechanism for fire spread into a WUI community is the transport of firebrands,

which are burning pieces of vegetation or structures that break off of whatever material is burning. They can cause spot fires that will directly ignite a structure or ignite nearby vegetation that can spread and subsequently ignite the structure, if combustible materials are present. As firebrands are the least understood of the three exposure conditions, research is needed to understand the mechanisms of firebrand production.

1.2 Motivation

Figure 1.2 shows historical data on the number of structures burned in wildfires each year in the United States and indicates an average of 2,000 to 3,000 homes damaged per year. Case studies of past fires have found that firebrands are the leading cause of home ignitions in the WUI, and they are cited for at least 50% of ignitions, if not more. The 2007 Grass Valley fire in Lake Arrowhead, CA destroyed 199 homes. Of those 199, 193 were thought to be ignited due to firebrand attacks, because the areas around the homes were clearly untouched by fire [5]. Studies of the 2007 Witch Creek and Guejito fires in San Diego County, CA also found that firebrands are a danger to communities with an estimate of at least two-thirds of the structures lost as a result of firebrands [6]. Although it is evident that firebrands play a large role in fire spread and the destructiveness of a WUI disaster, there is limited research on firebrands and their processes.

The issue of firebrands can be broken down into three processes: generation, transport, and ignition. Of these three processes, firebrand transport has received

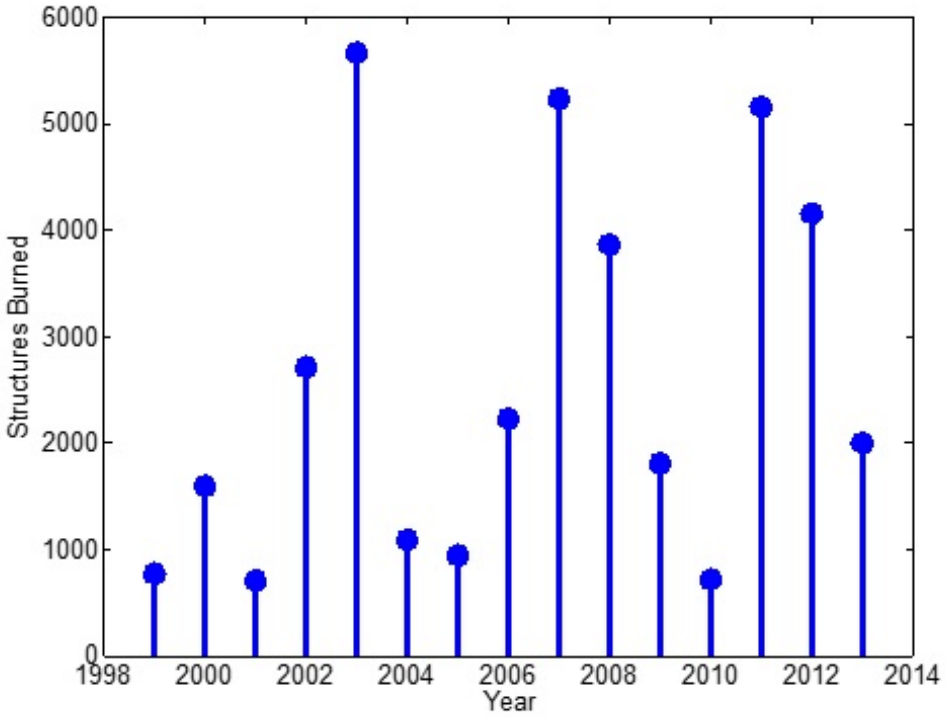

Figure 1.2: Data on structures burned in the United States due to wildfires shows that an average of 2,000 to 3,000 structures are burned per year [1].

the most attention. It is known from case studies that firebrands can be lofted large distances to ignite new spot fires and there is a large body of work in the literature on modeling the lofting and transport process. Although firebrand ignition of fuel is a very complex and stochastic process, there has been an effort to understand the ignition of fuel beds and some structural components, i.e. roofs and decks, from firebrands. There are also studies on the generation of firebrands, but almost all of these experiments are focused on collecting firebrands downstream to determine size (area and mass) and distribution of typical firebrands. A detailed summary of previous studies conducted on the firebrand processes discussed can be found in [1]. However, what is missing is knowledge on how and when firebrands are generated

or break off of the burning material.

The research that has been conducted on sizes and shapes of firebrands can be used to help in modeling the transport process, because sizes and shapes were previously just assumptions. Yet, there is still a need to relate the size of the firebrand to the initial size of the fuel. This would allow for a prediction of firebrand sizes to be made specific to a certain area depending on what types and sizes of fuel are burning. There is also a lack of scientific knowledge on how the firebrands break from the main fuel. The fuel is burning, which causes the structural properties of the fuel to change. Combustion of the fuel results in mass loss and density change and ultimately, a specimen that has lost a portion of its original strength. Wildland fires are accompanied by high wind speeds; these winds can produce so many firebrands that they are often called "firebrands showers" [7]. This means there must be a correlation between generation of firebrands and the wind speeds to which they are exposed. If a relationship can be drawn between the effect of combustion on the structural properties of the fuel and the drag forces induced by wind, it would aid in the prediction of when and what type of firebrands are produced during a fire. Understanding the mechanisms of firebrand breakage on the small scale will aid in the development of numerical models to better simulate fire spread in the WUI and determine an estimated firebrand flux for specific vegetation under given fire conditions. This knowledge can be coupled with the research of firebrand lofting and the probability of ignition of WUI fuels to develop detailed predictions of WUI fire spread scenarios. Additionally, this knowledge will be able to aid fire managers in decision making on what areas are most vulnerable under various fire and wind

conditions.

1.3 Research Objectives

The purpose of this thesis is to address the gaps discussed above in the research of firebrand generation. The focus of the current research is only on the generation of firebrands from wildland fuels, not firebrands that are produced from structures in the WUI. Experiments were conducted to better understand the effects of thermal degradation of wooden dowels at the small scale in order to determine the primary characteristics responsible for breakage. Various wood species and sizes were used to understand the effect of the initial properties of the vegetation on breakage mechanics. Figure 1.3 shows a flow chart that describes the three parameters that affect firebrand breakage: vegetation, fire, and wind. Initial physical properties of the dowel need to be quantified, because this is the information that is available before a WUI fire event takes place. The fire creates an updraft due to buoyancy, which results in a vertical buoyant force, F_B, and can cause breakage. The heat and combustion processes of the fire lead to degradation of vegetation, which results in mass loss and property changes, that can weaken it and cause fracture. Lastly, the winds that occur during a wildfire event have a velocity, U_W, that creates a drag force, F_D, which is another source of breakage.

The change of mass, volume, and density, which are all measured, gives insight to the burning process and the loss of strength that has occurred from thermal degradation. The mass loss rate of the dowels is another variable being measured that

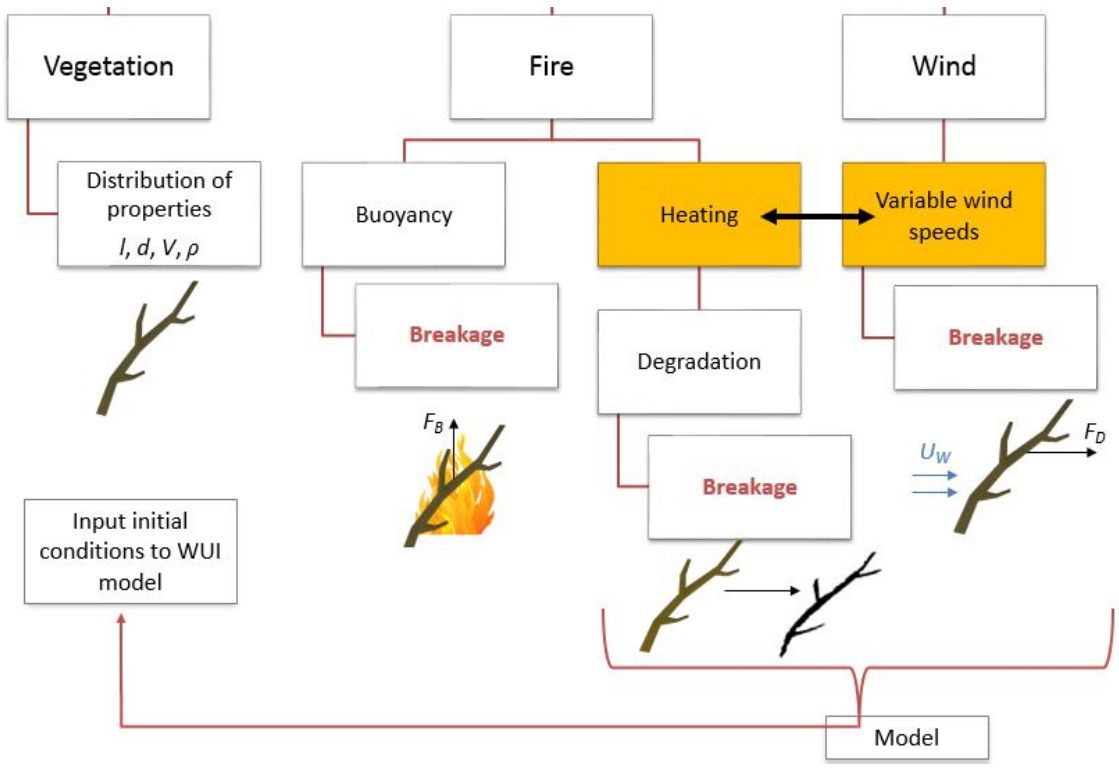

Figure 1.3: Breakdown of the three main parameters affecting firebrand generation to show how their interaction can be used to formulate a model of breakage criterion for initiating WUI spread models.

is necessary to relate the burning process to the physical and mechanical changes in the dowel. Failure mechanics are dependent on the strength and mechanical properties of the wood, so three-point bending tests were performed to measure the maximum force and deformation of unburned, or virgin, and burned dowels. This type of test was performed, because the loads applied to vegetation during a WUI fire that were discussed above create a bending moment, which can be measured by the three-point bending test configuration. The three-point bending tests allow for stress-strain curves for each experiment to be calculated, which gives insight into the types of failure behavior occurring. In addition to maximum stress and strain,

modulus of elasticity and modulus of rupture are other material properties that can be measured to quantify the strength of the material.

Non-dimensional scaling can be used to find a common trend that relates the failure mechanics to the thermal degradation of the dowels. This is the first step needed to formulate a firebrand breakage model. There also needs to be a connection made between the failure mechanics after heating and the wind speeds that are induced during a WUI event. The results of the breakage experiments are used to predict the magnitude of wind speeds that would be needed to result in the fracture forces measured. As shown in Figure 1.3, combining the effects of heating and the wind will create a comprehensive model of the breakage mechanics of firebrands in a WUI fire.

Chapter 2: Literature Review

2.1 Failure Mechanics and Properties of Wood

Wood is an orthotropic material, meaning that it has properties that vary along three orthogonal axes, and it is constructed of individual fibers forming annual growth rings, which result in growth in diameter. Because of these two features, its mechanical properties are dependent on the axis of growth. Figure 2.1 shows the three axes of wood, longitudinal, radial, and tangential, for a differential cross sectional area. The longitudinal axis is parallel to the grain; while, the radial and

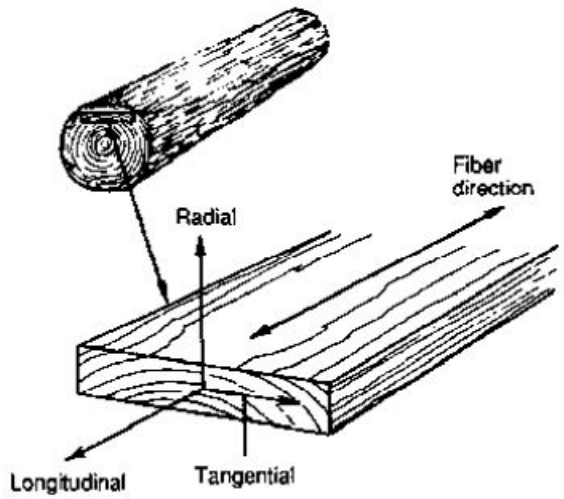

Figure 2.1: The three axes, longitudinal, radial, and tangential, with which wood mechanical properties vary [8].

tangential axes are perpendicular to the grain. The radial direction is defined normal to the growth rings, and the tangential direction is tangent to them. According to Ritter, "the differences between the radial and tangential directions are normally minor compared to their mutual differences with the longitudinal direction" [8]. Therefore, mechanical properties of wood are often only defined for the directions parallel and perpendicular to the grain.

Trees are divided into to groups: hardwoods and softwoods. These descriptions can be confusing, because they do not necessarily give an accurate description of the hardness of the wood. For example, longleaf pin and Douglas fir, which are two softwood species, are typically harder than basswood and aspen, which are hardwoods [9]. Botanically, hardwoods are angiosperms, and softwoods are gymnosperms or conifers. They also differ in their component cells. Hardwoods have pores and vessel elements; whereas, softwoods do not have vessel structures. The chemical composition of hardwoods and softwoods is also different, which affects the relative thickness of the char layer when it is formed [9].

Unlike steel, wood strength and ductility are different in tension and compression [10]. Figure 2.2 shows different loading configurations of wood and the typical failure mechanism associated with each. Wood in tension parallel to the grain experiences stretching of the wood cells, and the failure occurs due to cell-to-cell slippage or cell wall failure [8]. When compression is applied parallel to the grain, the stresses produced deform the wood cells along the longitudinal axis by shortening them. The failure in this case occurs from crushing of the cell structure [8]. Wood is comparatively strong in tension parallel to the grain, in contrast

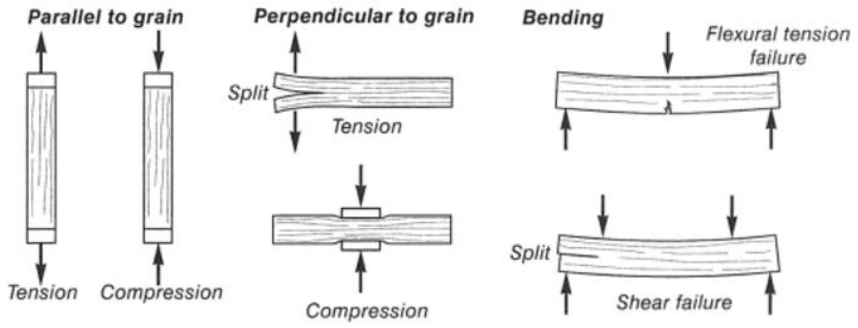

Figure 2.2: Possible loading scenarios depending on the type of loading, tension compression, or bending, and the direction of application, parallel or perpendicular to the grain (from [10]).

to tension perpendicular to the grain. Tension applied perpendicular to the grain separates wood cells perpendicular to their longitudinal axis, which causes the wood to split. When compression is applied to wood perpendicular to the grain, it causes the wood cells to deform perpendicular to their length leading to cell collapse [8].

When wood is subject to tension in either direction, it undergoes a brittle failure because there is no load sharing within the wood. In other words, as soon as a crack reaches a certain critical size, sudden failure will occur [10]. In this scenario, the wood exhibits linear elastic behavior until the point of failure. During compression loading, the wood also displays elastic behavior, when the load is first applied. The stress-strain relationship then becomes nonlinear, signifying that the behavior is no longer elastic and yielding is occurring. It will reach a maximum stress, and then will drop as the wood continues to be crushed [10]. Once the wood enters the plastic region, it deforms as a ductile material. These failure behaviors are represented by the stress-strain curve for clear wood given in Figure 2.3.

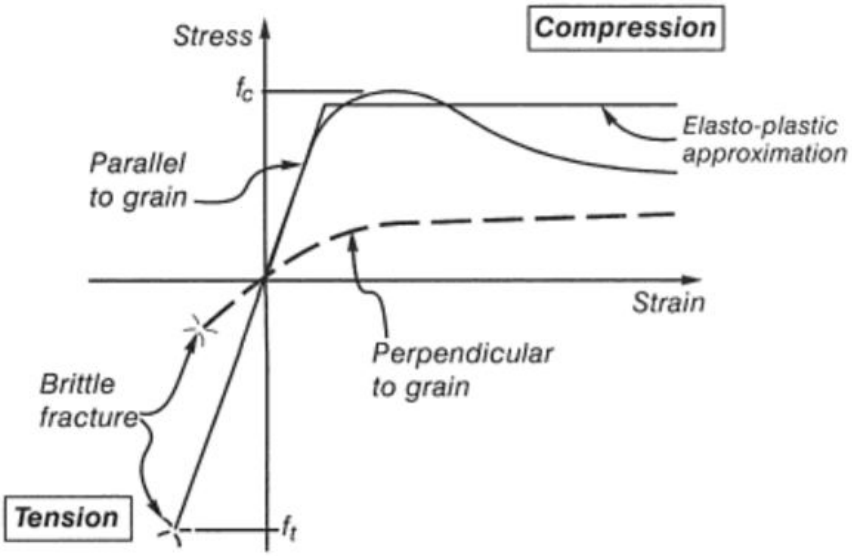

Figure 2.3: Stress strain curve for a wooden member subjected to compression or tension. The solid line is for a load applied parallel to the grain and the dotted line represents a load applied perpendicular to the grain (from [10]).

Wood subjected to bending experiences a combination of tension and compression behavior [10]. When a load is applied to a beam in bending, the side of the beam exposed to the load is subjected to compression, and the opposite side is in tension. This mechanism is shown in Figure 2.4, which also illustrates the shear forces induced during bending. The compression, tension, and shear forces are all parallel to the grain in this arrangement. If failure occurs from the shear stress, the wood will split along the grain. Alternatively, failure may result from the tension and begin to crack in this area, which can propagate all the way through the beam, as shown in Figure 2.2.

There are a variety of characteristics of wood that can affect its strength, even before heating. Some of these factors include density, slope of the grain, knots, rate

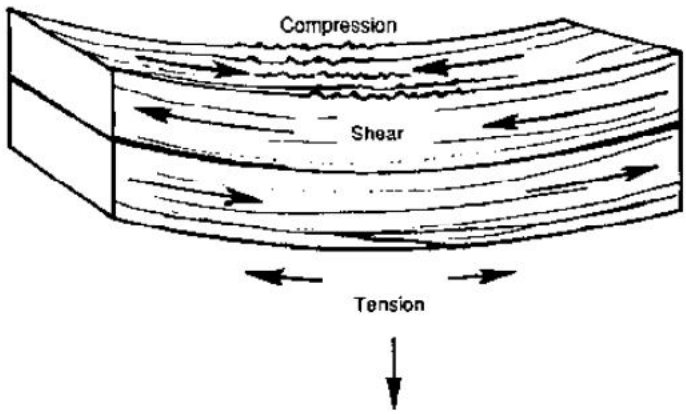

Figure 2.4: When a wood beam undergoes bending, it experiences compression, shear and tension forces acting parallel to the grain (from [8]).

of growth, and moisture content [11]. Failure stresses also depend on the size of the test specimen [10]. Van Casteren [12] explains that density is a critical factor controlling the mechanical properties of wood and that both longitudinal strength and stiffness are directly proportional to density. Straight-grained material will be stronger than materials with diagonal grain, or cross grain [8]. Wood with severe cross grain is also more likely to warp and have large knots, which are known to weaken the material from creating discontinuities. Because wood develops annual growth rings resulting in layers of wood with differing properties, the rate of growth can affect strength properties. Experiments have found that for most species there is a critical growth rate that will result in the greatest strength [11]. It has been found that strength and stiffness will decrease, when wood absorbs moisture and that these properties will increase, when the wood is dried below the fiber saturation point [8]. The fiber saturation point is defined as the moisture content above which the physical and mechanical properties of wood do not change as a function of

moisture content, and this value is approximately 30% for most woods [9]. Figure 2.5 shows the effect of moisture content on various strength properties of the wood.

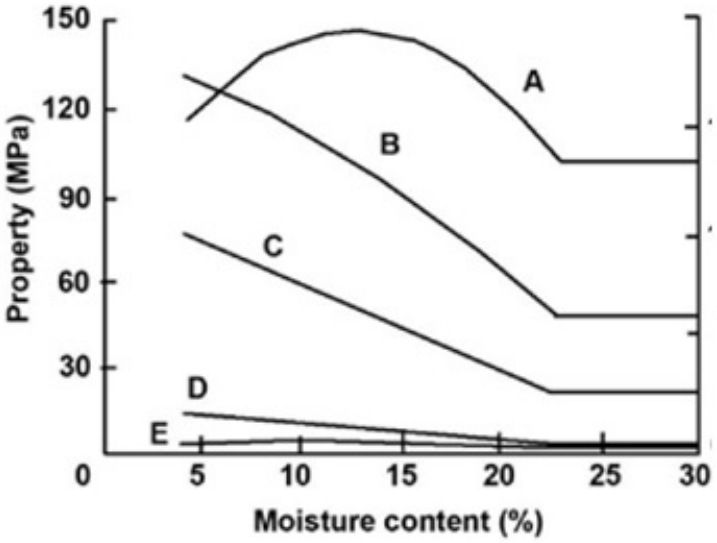

Figure 2.5: The effect of moisture content on tension parallel to grain (A), bending (B), compression parallel to grain (C), compression perpendicular to grain (D), and tension perpendicular to grain (E) (from [9]).

Natural fuels in the WUI can be thought of as branches with fractal geometry that are loaded with forces from weight and drag, if wind is present [13]. The loading configuration, therefore, can be described as a cantilever beam with an applied load at the middle of the beam from the weight and a uniform applied load across the length of the beam from the drag force induced by the horizontally applied wind. These loading configurations will result in bending of the beam as a result of the moments from the loads, which means that both tension and compression are occurring. The bending moment from the weight is only a function of the mass and

length of the dowel, but the dowel characteristics and wind speed and direction will all affect how the wind will deflect the dowel.

According to the Beaufort Wind Scale, which is used for hurricanes, twigs break at 39 mph - 46 mph (17 m/s - 21 m/s) and small and medium sized branches break at 47 mph - 54 mph (21 m/s - 24 m/s). There is no quantitative description of twigs verses small or medium sized branches, but this can give qualitative insight to the wind strength needed to cause failure without fire conditions present. Similarly, a scale is used to link the damages caused by tornadoes to wind speeds using the Fujita Scale, which associates branches breaking off trees with wind speeds between 40 mph and 72 mph (18 m/s and 32 m/s). During WUI fires, wind gusts can occur up to 69 mph (31 m/s) [14] depending on the fire and local weather conditions. The type of fuel and the season in which the fire occurs will influence the effect of the wind, because the surface area of leaves or needles on branches catches the wind and increases drag forces in canopies [15]. A study by Luley [16] on the effect of wind gusts on branches in Rochester, NY found that leafy months saw more branch failures, even though they did not necessarily experience larger wind gusts. During the leafy period, it was also found that few significant branch failures occurred when wind speeds were less than 40 mph (17.9 m/s) and that most branch failures were caused by gusts greater than 50 mph (22.4 m/s) [16].

Modulus of elasticity, E, and modulus of rupture, MOR, are two mechanical properties of wood that are related to bending mechanics. The modulus of elasticity is a measure of material stiffness and is defined by a ratio of material stress divided by strain. It can be found by calculating the slope of the linear, or elastic, portion

of a stress-strain curve. High values of modulus of elasticity mean that the material is stiff and not easily deformed elastically. Values for the modulus of elasticity can be measured for all three axes, E_L, E_R, E_T, representing longitudinal, radial, and tangential, respectively, through compression tests, but E_L is most often determined from bending tests [9]. The modulus of rupture represents the maximum load-carrying capacity of a member in bending, so it is synonymous with the ultimate or maximum stress. MOR is a description of the strength of a wooden beam, because it is a function of the maximum force that it can withstand before plastic deformation [9]. The size of the material and the method of loading will both affect the MOR. The strength of a material will decrease as size increases, as explained by the statistical strength theory [9]. This theory is applied to two beams with two equal loads applied symmetrical to the midspan points and allows for the ratio of modulus rupture of beam 1 to the modulus of rupture of beam 2 to be given by

$$\frac{MOR_1}{MOR_2} = \left[\frac{h_2 L_2(1+\frac{ma_2}{L_2})}{h_1 L_1(1+\frac{ma_1}{L_1})}\right]^{1/m} \tag{2.1}$$

where MOR is modulus of rupture, h beam depth, L beam span, a distance between loads placed $a/2$ each side of midspan, and m a constant. This theory allows for predictions of the ultimate strength of a material based on its physical properties to be determined and is useful because MOR can be used as a comparative measure of strength among various wood species.

2.2 Combustion Processes of Wood

Combustion of a solid fuel, like wood, involves many elementary chemical reactions, but these reactions can be lumped into two main processes: pyrolysis and oxidation. At temperatures slightly above 100°C, excess water is evaporated out of the wood. Temperatures between 200°C and 280°C induce reactions that are endothermic; there are gaseous products produced at this time that are non-combustible [17]. Pyrolysis is the first reaction to occur during the combustion process. When wood is heated to temperatures around 300°C, active pyrolysis begins [18], which produces pyrolysate gases, char, and ash. The pyrolysate and the char produced during the pyrolysis reactions are both susceptible to oxidation [19]. Oxidation of the pyrolysate is a gas phase reaction between the pyrolysate gases and the oxygen in the air. This homogeneous gas-phase reaction results in flaming combustion. The char can also go through oxidation, which can be described as a heterogeneous reaction involving the solid char and oxygen gas. This reaction results in smoldering combustion, because a solid material is undergoing oxidation. The following equations taken from [19] show very simplified chemical reactions for pyrolysis and the two possible oxidation reactions:

Pyrolysis:

$$Fuel\,(solid) + Heat \rightarrow Pyrolysate\,(gas) + Char\,(solid) + Ash\,(solid) \tag{2.2}$$

Gas-phase Oxidation:

$$Pyrolysate\,(gas) + O_2\,(gas) \rightarrow Heat + CO_2 + H_2O + other\ gases \tag{2.3}$$

Heterogeneous oxidation:

$$Char\,(solid) + O_2\,(gas) \rightarrow Heat + CO_2 + H_2O + Ash\,(solid) \tag{2.4}$$

These equations illustrate that pyrolysis must occur first in the sequence of reactions to produce pyrolysate and char. It is important to notice the differing products for smoldering combustion (heterogeneous oxidation) and flaming combustion (gas-phase oxidation), because smoldering combustion produces ash in addition to the typical products of combustion. This definition of pyrolysis is characterized by thermal degradation of the wood and an endothermic reaction; while, the two oxidation reactions are defined as exothermic reactions [19].

Zones develop through the wood surface when a piece of wood is heated in air due to the applied temperature gradient. Because wood has a relatively low thermal conductivity and density and a relatively high specific heat compared to other materials, the zones are well defined [17]. Figure 2.6 (adapted from [10]) shows a cross sectional view of a piece of wood that has been heated. The original surface has been reduced to a char layer, farther into the member there is a section of heated wood, and then there is a portion of wood that is still at the initial temperature. The piece of wood depicted in Figure 2.6 has been heated to the point of pyrolysis and chemical decomposition. There could be flaming combustion occurring, if the pyrolysate gases are burning; however, if oxidation is taking place in the char layer, smoldering combustion would be present. Smoldering combustion experiences lower temperatures, spread rate, and power compared to flaming combustion [19]. Typical temperatures for smoldering are in the range of 400°C - 700°C, and effective heat

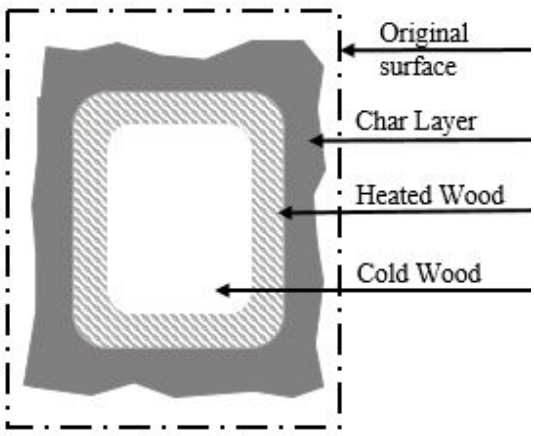

Figure 2.6: As wood is heating, distinct zones are developed. The original surface degrades to a char layer, which covers a zone of preheated wood, and unheated wood is in the center (adapted from [10]).

of combustion is usually about 6 kJ/g - 12 kJ/g when taking into account the combustion efficiency [19]. These values can be compared to 1500°C and 16 kJ/g - 30 kJ/g, which are typical flame temperatures and effective heat of combustion values, respectively, for flaming combustion [19]. Rein also explains, "smoldering spreads in a creeping fashion, typically around 1 mm/min, which is two orders of magnitude slower than flame spread" [19].

Charring rate, which is affected by the density and moisture content of wood, external heat flux, and oxygen concentration of the surrounding air, is a critical factor to determine fire endurance of wood members for construction purposes [18, 20]. Majority of rate of char data is obtained from exposing wood members to the standard time temperature curves of fire resistance tests like ASTM E119 and ISO 83. Figure 2.7, from [10], shows that charring rate decreases in a linear fashion with

increasing density and that the moisture content of the wood is another controlling parameter in this process. Sinha et al. [21] present several studies that have modeled

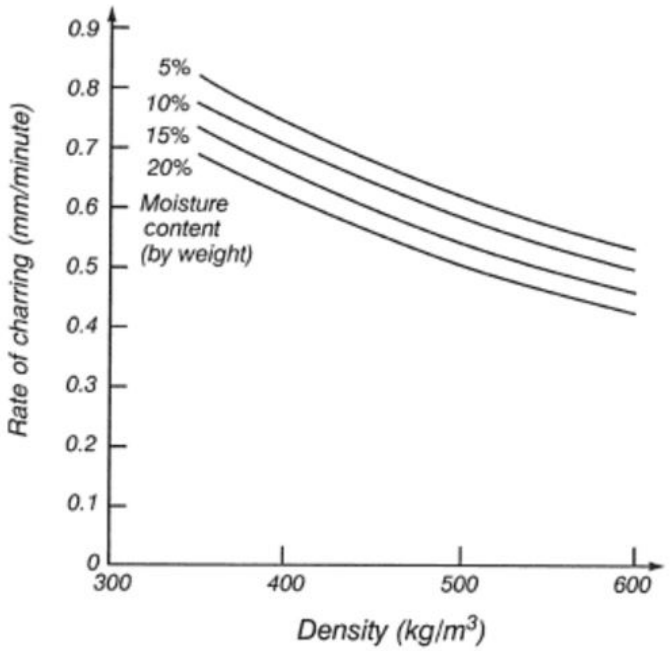

Figure 2.7: The effect of density and moisture content on the charring rate of wood (from [10]).

[22–24] and experimentally verified [20, 25] the effect of reduced cross-sectional area from heating on wood properties. The charring rate is found to be proportional to the external heat flux over the density of the wood, and temperature profiles within the uncharred wood can be represented by an exponential function [20].

Temperature changes can have either a reversible or irreversible effect on wood. When wood is heated or cooled quickly and then tested under those conditions, there is an immediate, reversible effect on the mechanical properties of the wood. This effect is generally a linear relationship between decreasing mechanical properties, namely modulus of elasticity, modulus of rupture, and compression parallel to grain,

and increasing temperatures [9, 26].

The irreversible effect on the properties of wood caused by increased temperatures for extended periods of time has also been studied. The permanent effect occurs due to degradation or mass loss of the wood. Green and Evans [27] studied the effect of cyclic and continuous long-term temperature exposure of 82°C on pine and Douglas fir samples. In all cases, the effect of cyclic temperature exposure on MOR was less than the effect of continuous exposure. Continuous exposure of 82°C for 30 months resulted in a 40% loss of MOR for both species tested [27]. Sinha et al. [21] also studied the effect of temperature on MOR and found that after exposure to 200°C for 2 hours, the MOR of all materials tested, Douglas fir and Aspen, decreased between 18% and 61%. Figure 2.8 shows the effect of oven heating at various exposure temperatures and exposure times on the modulus of rupture (left) and modulus of elasticity (right). These tests were conducted with oven dried (MC = 0) hardwood and softwood species. Higher temperatures cause a more dramatic decrease in both mechanical properties over a shorter period of time than lower temperatures with longer times of exposure. If modulus of elasticity and modulus of rupture are both affected when wood is heated, the stress-strain curves of heated wood will also be affected. Figure 2.9 shows derived stress-strain relationships by König and Walleij in 2000 from modeling results of bending tests performed by König in 1995 [10]. These curves are simplified and can be used as a method of predicting possible failure behavior. For example, they show that the modulus of elasticity and modulus of rupture both decrease with increasing temperature.

Thermal properties of wood also have a dependence on temperature. Accord-

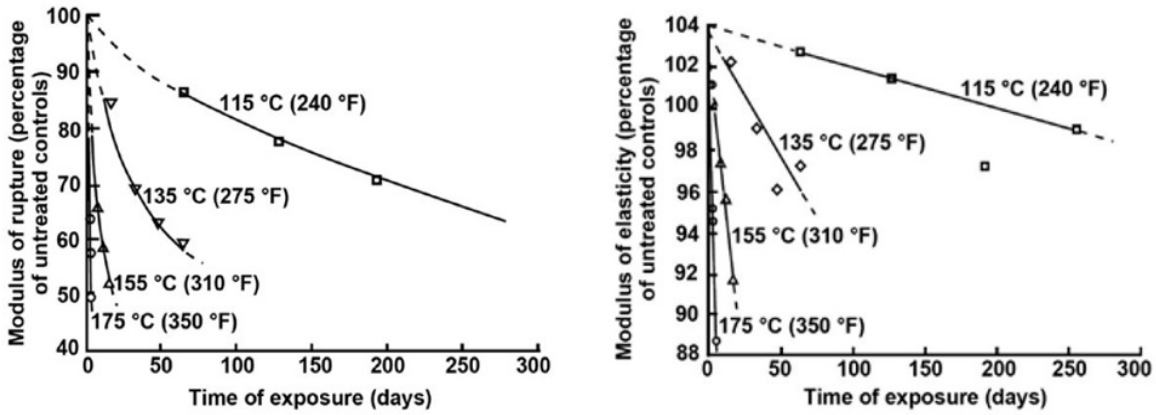

Figure 2.8: Modulus of rupture (left) and modulus of elasticity (right) as a function of various exposure temperatures for different durations (from [9]).

ing to Buchanan, "density drops to about 90% of its original value when temperature exceeds 100°C, and to about 20% of its original value when the wood is converted to char above 300°C" [10]. The thermal conductivity experiences a rise until about 200°C, followed by a decrease to about 350°C, and finally a steady increase again to about 1000°C, as shown in Figure 2.10 on the left, because of the various components that react at different temperatures. There is a sharp increase in specific heat around 100°C due to the heat required to evaporate the water, which has a very high specific heat, from the wood, as illustrated in Figure 2.10 on the right. After this point, the specific heat decreases until about 400°C where it begins to even out. These properties will affect conductive and convective heat transfer, respectively.

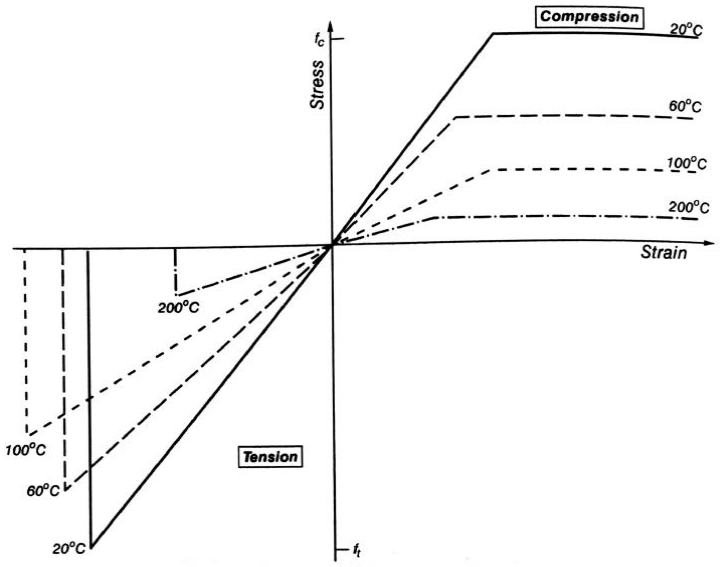

Figure 2.9: Stress-strain curves for wood in tension and compression when heated to various temperatures (from [10]).

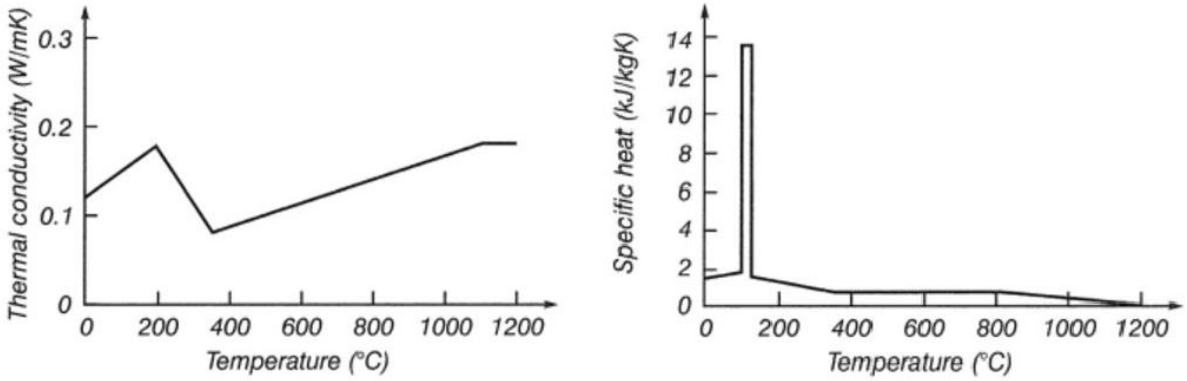

Figure 2.10: Thermal conductivity (left) and specific heat (right) variations as a function of temperature (from [10]).

2.3 Firebrand Breakage

The majority of firebrand generation studies in the literature are mostly focused on collecting firebrands produced from vegetation, structural components, full

scale structures, and WUI fires to observe size and distribution. For vegetative fuels, Manzello et al. [28] studied firebrand generation from Douglas fir trees that were 2.6 m and 5.2 m tall and ranged from 10% - 50% moisture content. Approximately 70 firebrands were collected in water pans and then dried from each tree. There was no wind applied during the tests, and it was found that no firebrands were produced if the moisture content of the trees was greater than 30%. All firebrands that were

Figure 2.11: A sample of firebrands, which are cylindrical in shape, collected during experiments by Manzello et al. [28].

collected in these experiments were cylindrical with an average diameter of 3 mm and length of 40 mm for the 2.6 m tall tree and 4 mm diameter and 53 mm long for the 5.2 m tall tree. Figure 2.11 shows a picture of a sample of the firebrands collected. The firebrands from both tree sizes were also similar in mass with a high majority of firebrands collected weighing less than 0.3 g. Manzello et al. [29] performed similar experiments as [28] but with 4 m tall Korean pine trees instead of Douglas fir trees. These experiments also produced solely cylindrical firebrands of similar size and mass. The average firebrand diameter from the Korean pine trees was 5 mm and 40 mm in length. Figure 2.12 shows the mass distribution of the

experiments conducted by Manzello et al. [28, 29] side by side.

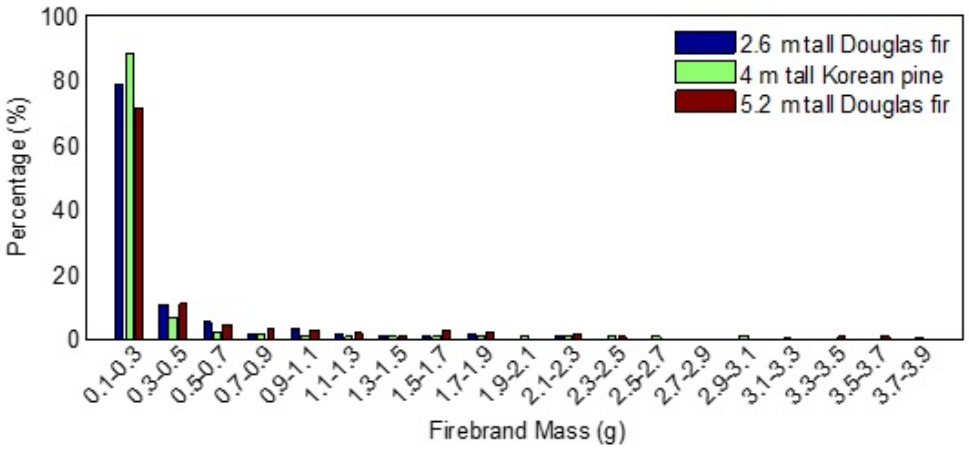

Figure 2.12: Experiments by Manzello et al. [28, 29] found that the majority of firebrands produced from Douglas fir and Korean pine trees of various sizes were 0.1-0.3 g (from [1]).

There are also a variety of studies that focus on firebrand generation from structural components and full size structures. Waterman [30] was one of the first to study this phenomena by studying firebrand generation from burning wood shingle roof constructions. The majority of firebrands collected from these studies were disk shaped [1]. Vodvarka [31, 32] and Suzuki et al. [33, 34] both studied firebrand production from full scale structures under various conditions. Like in studies with vegetative fuels, small firebrands dominated the majority of what was produced. Most firebrands collected by Vodvarka [31, 32] had an area smaller than 0.23 cm^2. Tests performed by Suzuki et al. [33] found that above 95% of firebrands collected in the structure burns were less than 10 cm^2 in projected area when collected 18 m from the structure and 4 m from the structure. Suzuki et al. [33, 34] also found that

firebrands produced from individual structural components have sizes very similar to those collected from full scale buildings, which demonstrates that information from small scale experiments is valuable.

Size distributions of firebrands have also been measured in real WUI fires. The first study of this kind was during the Angora fire in California in 2007 [35,36]. The main fuel types present in this fire were white fir and Jeffrey pine, and the surface fuel loading could be characterized as heavy understory [37]. Data was collected post fire by analyzing holes that were created in a trampoline from brands melting the canvas of the trampoline. A total of 1,800 burn holes were photographed and analyzed, which resulted in finding that 95% of the burn holes had an area of less than 1 cm^2, whereas the largest burned area was 10.3 cm^2. Burn patterns were also observed on building materials and outdoor furniture at 212 different locations that were affected by the Angora fire. This information concluded that the largest indication of firebrand deposit was 2.02 cm^2, while the majority of firebrand burn spots was less than 0.4 cm^2.

Observations were made about firebrand size distributions after the Bastrop Complex fire, which occurred in 2011 in Texas, using the same technique as in the Angora fire study of measuring the sizes of burn holes in trampolines [38]. Fuel type present during this fire was Loblolly pine overstory with yaupon holly understory [38]. The data was taken at seven locations in the area affected by the fire, which allowed for a variety of conditions that could affect firebrand generation to be studied. The trampolines were located up to 30 m away from both vegetation and structures in areas that experienced low to high fire intensity and heading and

flanking fires. The canopy cover ranged from open to dense in the studied area. The size distribution of holes from firebrands is similar to what was measured after the Angora fire, as shown in Figure 2.13, with 90% of the holes less than 0.5 cm^2 in size.

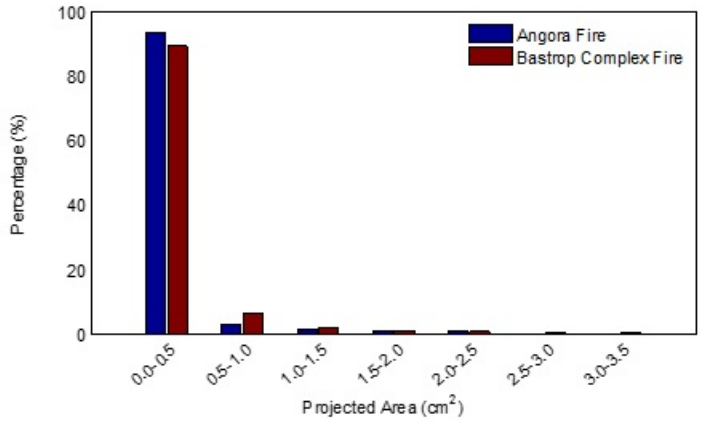

Figure 2.13: Distribution of the size of burn holes from firebrands on trampolines during the Angora [35,36] and Bastrop Complex [38] fires (from [1]).

Firebrand generation studies were also performed in the New Jersey Pine Barrens to characterize mass, size, and origin of firebrands in the field [39]. This is one of the first studies that incorporates the importance of characterizing and closely studying the sizes of the source fuel. Before the fire, fuels were classified into the typical 1-h, 10-h, and 100-h class ratings, where 1-hr fuels are defined as having a diameter less than 6.35 mm. The 1-hr fuels were further divided into subgroups to determine size of consumed particles at a higher resolution, as follows: S1 fuels were less than 2 mm in diameter, S2 fuels ranged from 2.01 mm - 4 mm in diameter, and S3 fuels ranged from 4.01 mm - 6.35 mm in diameter. Pine bark and shrubs were sampled during the tests to determine what size classes were breaking off to

become firebrands. The average horizontal wind speed was measured to be 1.8 m/s with a peak value of 6.4 m/s. A sample shrub, which had branches that experienced charring, partial burning, and total burning, was analyzed pre- and post-fire and is pictured in Figure 2.14 to get a more detailed description of what is happening during a fire. After examining all the data, it was found that all branches in the S1 category on the sample shrub were consumed, S2 fuels were partially consumed, and fuels characterized as S3 were not consumed. 70% - 89% of firebrands collected from these experiments were slices of bark, and the remaining collected pieces were cylindrical pieces from branches.

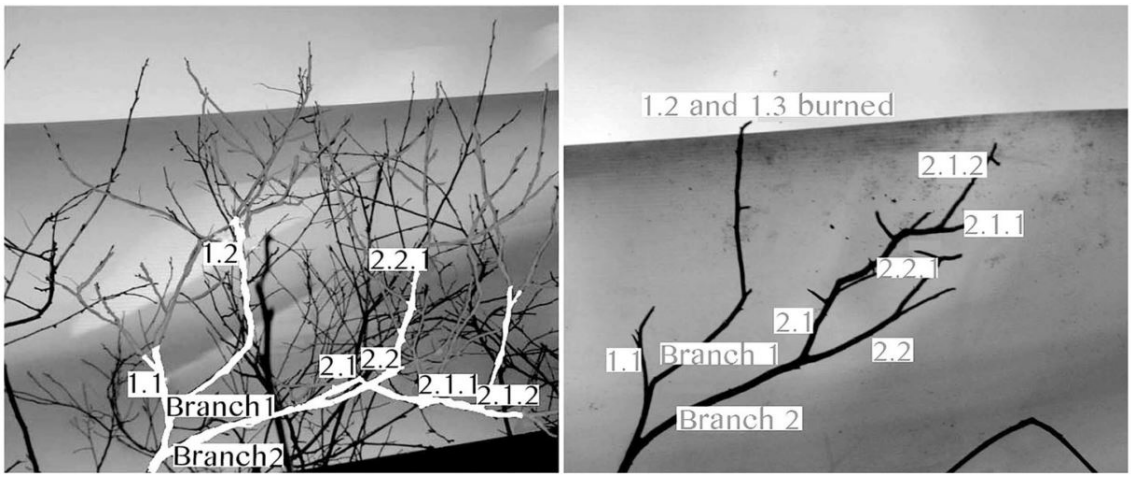

Figure 2.14: Pictures of a sampled shrub pre (left) and post (right) fire during an experimental study by Housammi et al. [39].

None of the studies discussed above have attempted to characterize or describe the physical processes and mechanisms of firebrand generation. Barr and Ezekoye [13] investigated breakage and subsequent lofting of firebrands via a thermal plume. They used a fractal model to describe wildland fuels and paired this with combustion

models, specifically concerning the oxidation process, to create inputs for numerical models. In these experiments, three-point bending tests were performed on Yellow poplar rods with diameters of 4.8 mm, 6.4 mm, and 7.9 mm. There were three conditions for the tested dowels: ambient conditions (14°C, 90% relative humidity), oven heated at 101°C for 1 hour, and oven heated at 250°C for 1 hour. None of the three scenarios represent real fire exposure, where pyrolysis and oxidation occur. The second condition represents the heating process of drying the wood to evaporate moisture, and the last condition resulted in mass loss due to both evaporation and the onset of pyrolysis. The results from these experiments show a somewhat linear trend between the flexural strength and density; however, the rate of change of the strength with respect to the density varies for the three different heating conditions.

Tohidi et al. [40] proposed a mechanical model for firebrand breakoff due to shear stress associated with an internal bending moment that exceeds the maximum bending moment the specimen can withstand. They developed a scale analysis using data from experiments by Manzello et al. [28, 29] with Douglas fir and Korean pine trees. The bending moment is created due to the material weight and drag forces, which can be produced in the vertical direction generated by buoyancy from the fire plume or the horizontal direction from ambient winds. These driving forces were combined to define a critical shear stress for breakage as:

$$\sigma_{max} = \sqrt{\left(\frac{8\rho_{air}C_D U_h^2 \eta^2}{\pi}\right)^2 + \left(\frac{8\rho_{air}C_D U_v^2 \eta^2}{\pi} - 4\rho_{wood} g L \eta\right)^2} \tag{2.5}$$

where ρ_{air} is the air density, C_D the drag coefficient, U_h and U_v horizontal and vertical components of the air velocity, respectively, η the aspect ratio ($\eta = L/D$),

and ρ_{wood} the density of the wood or fuel.

This is a simplistic model that does not account for charring or burning of the material, which causes degradation and weakening. From this model, it was determined that fuel with large aspect ratios (long and thing) are more susceptible to firebrand break off. When the material has a large aspect ratio, this means the dominating breakage mechanism is due to drag forces. If the material has a smaller aspect ratio, weight is the dominating breakage force. The studies by Barr and Ezekoye [13] and Tohidi et al. [40] both propose a beginning approach to include generation of firebrands into an initialization model, which has been missing up to this point. This information is necessary for better prediction of firebrand transport, and data needs to be collected to inform these models.

Chapter 3: Experimental Setup

3.1 Firebrand Properties

Experiments were conducted with cylindrical wooden dowels of three different wood species: oak, birch, and poplar. These species were chosen because they provided a wide range of material properties and could be machined into small wooden dowels. While firs and pines are species that are often used when studying WUI fuels, as discussed in Section 2.3, vendors were unable to machine these species into the shape and sizes requested because they are softwoods and would break in the process. As this study attempts to develop a framework for studying breakage, it was more important to have repeatable samples over a wide range of properties than using actual WUI fuels. In the future, twigs from actual WUI fuels can be analyzed using the same techniques.

Birch, oak, and poplar have a wide range of initial densities, 610 kg/m^3, 700 kg/m^3, and 540 kg/m^3, respectively. These are the average initial densities measured before testing. Because density is an important factor in the strength properties of materials [12] and Barr and Ezekoye [13] found a relationship between stress and density, it is necessary to study species with a range of initial densities. Density of Douglas fir and pine species, which are more typical in WUI fires, can range from

approximately 350 kg/m^3 - 530 kg/m^3. The lower end of densities tested overlaps with the higher end of densities of these typical WUI fuels.

The dowels were all cylindrical in shape and had diameters of 6.35 mm, 9.53 mm, and 12.7 mm (1/4 in, 3/8 in, and 1/2 in, respectively). Some tests were also performed using dowels with diameters of 3.18 mm and 4.76 mm (1/8 in and 3/16 in, respectively), but these sizes were only available for birch wood. These smaller sizes, however, were not used in all the heating methods, which will be discussed in the following section. Cylindrical shaped dowels were chosen because this is the shape primarily found during firebrand production studies involving vegetative fuels. Disk and spherical shapes have been reported but not as frequently as cylindrical shaped firebrands, and those shapes are usually produced from bark or structural fuels. This research is focused on production of firebrands from natural fuels that contain branching with no leaves or needles present. The reason for this is to start with modeling the simplest form of firebrand generation and to physically understand what is happening on the small scale. This research can be used as a framework that could be extended to fuels of different shapes or configurations, like branches with leaves and needles. The connection among combustion, mechanical properties, and breakage must be made for the simplest configuration before extending it to more complicated scenarios.

In a high intensity prescribed fire in the New Jersey Pine Barrens, it was found that branches with a diameter less 4 mm were either partially burned or completely consumed, but branches with a diameter greater than this were still attached to the shrub after the fire passed [39]. This fire spread predominately as a surface fire

through Pitch pine with scattered oaks in the overstory and an understory of mostly scrub oaks and huckleberry. The dowels used in this research range in diameter from 3.18 mm to 12.7 mm (1/8 in to 1/2 in). The smaller sizes did not produce useable data in all tests, which is why larger sizes were used. It should also be noted that the wind speeds during the Houssami et al. [39] experiments were 1.8 m/s on average, with a peak of only 6.4 m/s, which is low compared to severe WUI fire conditions. Drag forces induced by winds are one of the variables that can cause breakage, and this is a relatively low wind speed, which could explain why only branches with very small initial diameters were consumed during the previous study.

All of the dowels were cut to 10.2 cm (4 in) in length for the three-point bending tests. This length was solely determined by the size of the three-point bending apparatus. Moisture contents were measured with a moisture content analyzer and were found to range from 5% - 8% on a dry basis for all three species. Every test specimen was weighed on a precision balance (Tree Scales Model: HRB203) that is accurate to 0.001 g before each test. The initial density of each individual dowel tested was calculated from the initial mass and the initial volumes.

3.2 Heating Modes

Before performing strength tests on the dowels, multiple methods of heating were tested to determine how to create the most repeatable and realistic conditions. Because of the multiple parameters that are involved in the breakage process, it is important to develop a process that could be repeatable to ensure that all trends

found are accurate. At the same time, the heating method must be representative of what occurs during a fire. Initial experiments were performed in a small 12 cm x 16.5 cm x 11 cm (4.7 in x 6.5 in x 4.3 in) Thermolyne furnace (Type 1400), which has a dial for programming the internal temperature. Heating the dowels in the furnace was a difficult process for various reasons. In the furnace, the mode of heat transfer was convection, and it was able to produce enough heat for surface oxidation of the dowels to occur. Because there was a very limited supply of ambient air, the oxidation was increased and the dowels turned to char and ash very quickly. The char layer, which contains no strength, would consume the majority of the original cross-section of the dowels, which would become so brittle that no bending tests could be performed. This was not an accurate representation of the combustion processes that occur during a fire, which eliminated this method of heating.

Temperature is a useful way to characterize the heating process, so a programmable hot plate (Corning PC-600D) was used in place of the small furnace. Preliminary tests were conducted to observe the charring of samples to allow for a range of heating times that provided differing degrees of degradation to the samples to be determined. It was thought that a hot plate would perform better than the furnace, because it is open to ambient air, so it would slow down or prevent surface oxidation. There were two variables in these experiments that were controllable and changed, in order to see the effect each has on the degradation of the strength of the dowel. These two variables were temperature, which was set to 350°C, 375°C, or 400°C, and time of heating, which was either 10, 15, or 20 minutes. This temperature range was chosen because the average pyrolysis temperature of wood, 360°C,

is in this range. There was one set of tests performed at a constant temperature of 350°C with the heating times varied from 10, 15, and 20 minutes. The second set of tests conducted on the hot plate were all performed for 15 minutes, but the temperature increased from 350°C to 375°C to 400°C.These tests were performed on all five diameters of the birch dowels; however, the first set of hot plate tests were performed using birch (5 diameters), oak (2 diameters), and poplar (2 diameters). A detailed breakdown of these tests are given in Table 3.1.

Table 3.1: Overview of the heating mode, species, and diameter used in the three different groups of tests.

	Group 1	Group 2	Group 3
Heating Mode	Hot Plate Constant T= 350°C Times: 10, 15, 20 min	Hot Plate Constant t= 15 min Temps: 350°C, 375°C, 400°C	Propane Flame Flaming times: 10, 15, 20 s
Species	Birch (B), Oak (O), Poplar (P)	Birch (B)	Birch (B), Oak (O), Poplar (P)
Diameter (in)	1/2 (B) 3/8 (B, O, P) 1/4 (B, O, P) 3/16 (B) 1/8 (B)	1/2 (B) 3/8 (B) 1/4 (B) 3/16 (B) 1/8 (B)	1/2 (B, O, P) 3/8 (B, O, P) 1/4 (B, O, P)

When heating the dowels on the hot plate, heat conduction is the main mode of heat transfer. The hot plate consists of two heating elements with a ceramic cover, which causes temperature gradients across the surface. In order to equally heat the dowels around their entire circumference, the dowels were rotated every 3 minutes during all tests. Because the surface of the hot plate was not completely uniform in temperature, the dowels did not always experience reliable heating even

with the rotations. The dowels would produce pyrolysis gases, but there was no pilot, so there was no active combustion occurring. There was a production of a char layer, but because there was adequate ambient oxygen the temperatures did not reach high enough to sustain surface oxidation.

In order to simulate more realistic conditions of a WUI fire, a final heating mode was used prior to three-point bending tests. Dowels were exposed to a propane flame created by a large Bunsen- type burner to induce flaming combustion. The height of the flame was kept to approximately 23 cm (9 in) and the width of the base of the flame was about 9 cm (3.5 in). These conditions were kept as constant as possible for all tests, because the gas flow rate could not be measured with the regulator that was required to be used for the burner. Birch, oak, and poplar dowels were all used in these tests, and they were exposed to the flame for 10, 15 and 20 s. These times are defined to start as soon as the dowel ignites; therefore, they can be thought of as the time of flaming. These times were found to produce a range of effects on the diameters tested, even though they are short durations. The dowels were rotated in the flame every five seconds to create even heating on all sides of the dowel. All three species tested in these experiments used dowels of the same three diameters, as shown in Table 3.1.

The premixed propane flame produces higher temperatures than typical WUI fires experience, the adiabatic temperature of a propane flame burning stoichiometrically in air is about 1994°C (2267 K) [41], but this temperature and the flaming combustion is more realistic than heating conditions in an oven or on a hot plate. Although these tests created flaming conditions more similar to a real WUI fire

Figure 3.1: The burner used for flaming tests next to the nitrogen box used to extinguish any active combustion.

than the hot plate tests, the exposure times were small, and they did not allow for smoldering to occur. Surface oxidation was avoided in all experiments, so there were no complications with the three-point bending tests. In order to ensure that all pyrolysis stopped and the heating times were as accurate as possible, the dowels were placed in a 22.9 cm x 33 cm x 6.35 cm (9 in x 13 in x 2.5 in) aluminum box, which is shown in Figure 3.1 next to the burner. The box was lined with kaowool ceramic insulation fiber, so that the dowels would not fracture when placed inside and had nitrogen gas injected through an inlet hole in the top of the box. The nitrogen gas was used to extinguish any combustion processes, flaming or smoldering, that were still occurring. There was also a small outlet hole in the top of the box so that any

hot gases could be exhausted out. The mass of each specimen was again weighed on the precision balance, so that a change of mass and mass loss rate could be calculated for each dowel. Before performing the bending tests, the heated dowels were photographed so that any changes in length or diameter could be observed. The total time between placement in the nitrogen box and the bending tests ranged from fifteen to twenty minutes. This resulted in cooling of the dowels, which were approximately at room temperature during the bending tests. MATLAB was used to perform image analysis on the dowels, so that the properties of each dowel did not need to be measured individually after each test.

3.3 Three-Point Bending Tests

A PASCO Materials Testing System, shown in Figure 3.2, was utilized with the bending accessory to perform three-point bending tests on all of the heated dowels. There was also a set of three-point bending tests conducted with virgin dowels of all the species to produce data on initial mechanical properties. The bending accessory has a base to which two supports are screwed into and a plunger that moves in the vertical direction by using a hand crank. This creates the typical three-point bending test condition with a beam in a simply supported configuration and a single concentrated load applied in the center of the beam. The test specimen, or dowel, rests on the supports and the load is applied via the plunger descending onto the dowel. The length span between the supports, L_s, is measured to be 8.65 cm (3.4 in), which means that supports are each located 0.76 cm (0.3 in) from the edge of the 10.16 cm (4 in) long dowel.

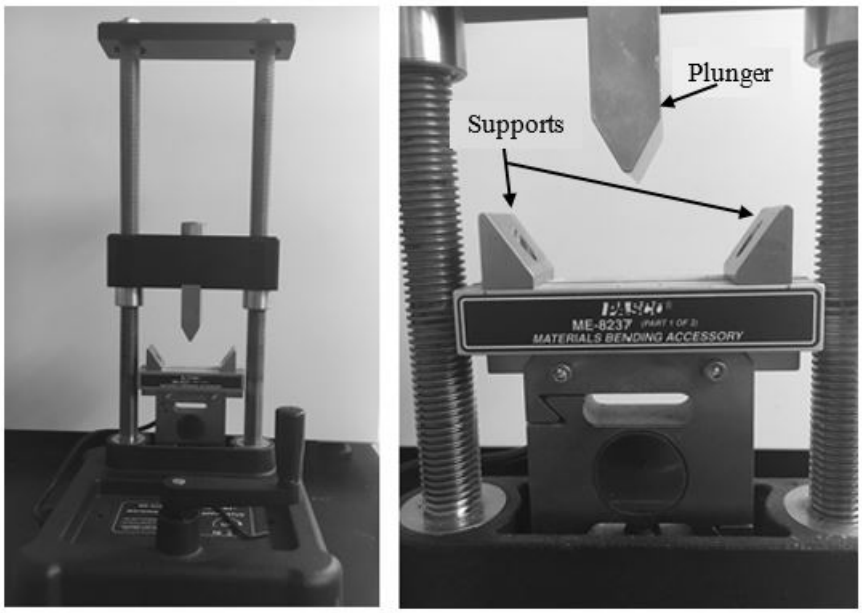

Figure 3.2: The Materials Testing System (left) and a close up of the three point bending accessory (right) with the supports and plunger labeled.

The Materials Testing Systems software measures the force applied to the specimen through the plunger by a 7,100 N load cell in the base of the machine. The position of the tip of the plunger is measured when the software is recording data by an optical encoder. The applied force and position of the plunger are measured as a function of time as direct outputs of these tests. The loading rate during the bending tests was approximately 90 mm/ min for all tests. From these measurements, stress and strain can be calculated for each test. An average of the individual stress-strain curves is used to obtain a single curve for each species, diameter, and heating condition. From the elastic, or linear portion, of the curve, Hooke's Law can be used to determine the average modulus of elasticity for each testing group. Along with visual observations of the breakage, the stress-strain curves allow for more insight to be gained on the breakage mechanism occurring,

whether it be a brash, abrupt failure or a fibrous fracture where the wood splinters apart.

Photographs are taken of each dowel after the bending test to distinguish the manner in which the dowels failed. The modulus of elasticity and the modulus of rupture can be compared for all the testing conditions, so that observations of how the variables affect the stiffness and strength can be made. Figure 3.3 shows a summary of the experimental procedures discussed in this section. A more detailed discussion of how these values are calculated, averaged, and their associated errors will be given in Section 4 of this thesis.

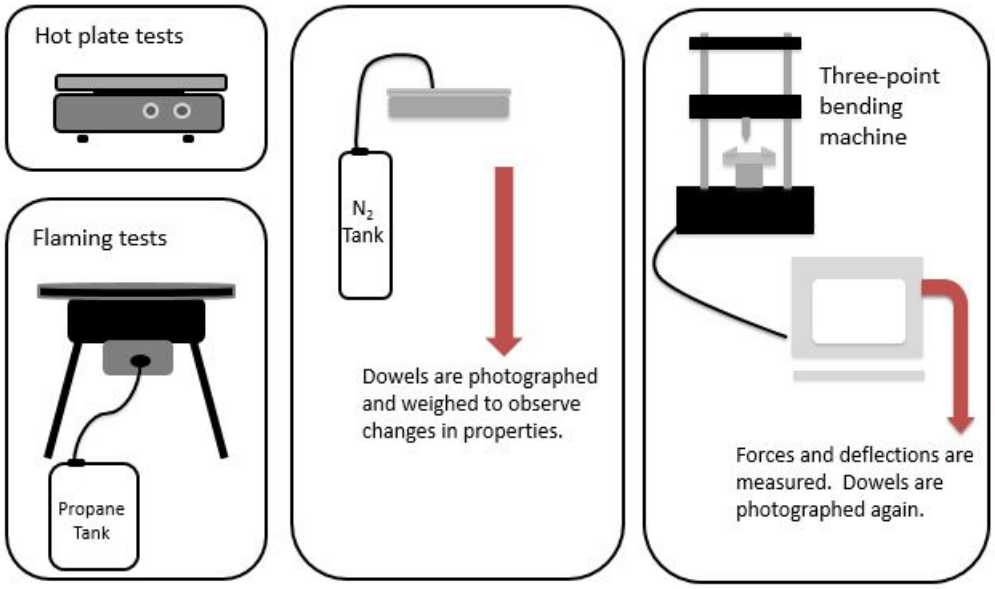

Figure 3.3: Summary of the experimental procedures discussed throughout this section. Dowels are weighed and then exposed to heating on a hot plate or in a flame. The heated dowels are placed in a nitrogen box to extinguish any combustion still occurring. The dowels are weighed again and photographed to observe changes. Finally, three-point bending tests are performed on the dowels to measure breakage properties.

Chapter 4: Results

4.1 Visual Observations

Comparisons between failure mechanisms between the two heating methods, the hot plate and the propane flame, were made through observations of the breakage of the dowels during the three-point bending tests to understand what breakage mechanisms were occurring during the different tests. Figure 4.1 shows photographs of 6.35 mm (1/4 in) diameter birch dowels that have been heated at 400°C for 15 minutes, 350°C for 15 minutes, 350°C for 20 minutes before the bending tests were performed. Comparing Figures 4.1(a) and 4.1(b) shows that increasing the temperature by 50°C causes much more degradation of the dowels where the fibers begin to break apart solely due to heating, which is seen in Figure 4.1(a). This characteristic of the dowels tested at high temperature resulted in some difficulties during bending tests. A comparison between Figures 4.1(b) and 4.1(c), which is much less drastic than the previous comparison between different exposure temperatures, shows the effect of increasing the heating time. It can be seen in Figure 4.1(b) that some of these dowels still have some visible virgin wood on the surface because they were only heated for 15 minutes in comparison to the 20 minutes of exposure experienced by the dowels in Figure 4.1(c), which are fully blackened on the surface.

The majority of the dowels that were heated with the hot plate experienced

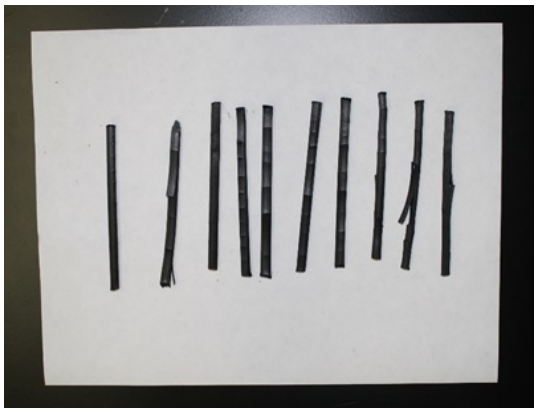

(a) Heated for 15 min at 400°C.

(b) Heated for 15 min at 350°C.

(c) Heated for 20 min at 350°C.

Figure 4.1: Photographs of 6.35 mm (1/4 in) diameter birch dowels after being heated on the hot plate. The differences of increasing temperature and time can be seen by comparing the three images.

fibrous breakage during the three-point bending tests. The splintering of the fibers during this type of breakage often occurred at a 45°angle, and the location of the applied force was obvious because the dowels did not snap into pieces. An example of this breakage mechanism is shown in Figure 4.2, which is a photograph of 9.525 mm (3/8 in) diameter oak dowels after bending tests were performed that have been exposed to a temperature of 350°C on the hot plate for 15 minutes. There was one instance here were the dowel tested completely split, but the remainder of the dowels show fibrous fracture on the side of the dowel that was in tension during the test. This breakage mechanism was dominant for all three species. However, birch dowels were tested with a larger range of diameters, and it was found that 4.76 mm (3/16 in) diameter dowels had an even distribution of the two breakage mechanisms than dowels with larger diameters. Figure 4.3 shows that a little over half (six out of ten) of the 4.76 mm (3/16 in) diameter birch dowels exposed to 350°C for fifteen minutes experienced fibrous failure, while the remainder resulted in a clean break

Figure 4.2: Photograph of oak dowels of diameter 9.525 mm (3/8 in) heated on the hot plate for 15 min at 350°C after bending tests.

Figure 4.3: Photograph of birch dowels of 4.76 mm (3/16 in) diameter heated on the hot plate for 15 min at 350°C after bending tests.

of the dowel into multiple pieces. The dowels tested with diameters below 4.76 mm (3/16 in) had mostly brash failures ending with the original dowel broken into at least two pieces. This shows that it is evident that the size of the dowel contributes to the mechanics of the breakage; but, it is not clear if the transition occurs for all species at a similar size, because oak and poplar were not tested on the hot plate with diameters in the lower range.

In the tests with a propane flame as the heat source, there is a wider range of breakage mechanisms over shorter exposure times. For example, Figure 4.4 shows the results after the bending tests for 6.35 mm (1/4 in) diameter birch dowels after 10 s and 20 s exposure. In this case, the 10 s exposure resulted in a fibrous fracture for the dowels (4.4(a)), but after 20 s exposure the dowels all failed in a brittle manner (4.4(b)). The 15 s burning time of this size dowel produced a mixture of the two breakage conditions. The three-point bending tests on the oak dowels of this size resulted in the same trend as the birch. Brash, complete failure was observed for

(a) Breakage after 10 s flaming time. (b) Breakage after 20 s flaming time.

Figure 4.4: Photographs of 6.35 mm (1/4 in) diameter birch dowels with 10 s (a) and 20 s (b) flaming times. Two different breakage mechanisms occur: fibrous (a) and abrupt (b).

the 6.35 mm (1/4 in) diameter poplar dowels at all three time exposures, however. Figure 4.5 shows that even after a burning time of only 10 s the majority of the 6.35 mm (1/4 in) poplar dowels broke into pieces through abrupt failure.

The two larger diameters 9.525 mm and 12.7 mm (3/8 in and 1/2 in, respectively) were observed to break in the fibrous method, with fractures occurring at 45°angles and fibers splintering apart, for all three species even when the exposure time was 20 s. These tests also show that the size of the dowel is a controlling factor of the breakage mechanism, in addition to the exposure time, which was not as clear in the hot plate tests. Not only did the flaming tests allow for more realistic fire conditions to be achieved in a repeatable manner, but they also allowed for a wider distribution of breakage mechanisms to occur for the given species over the same amount of changing variables.

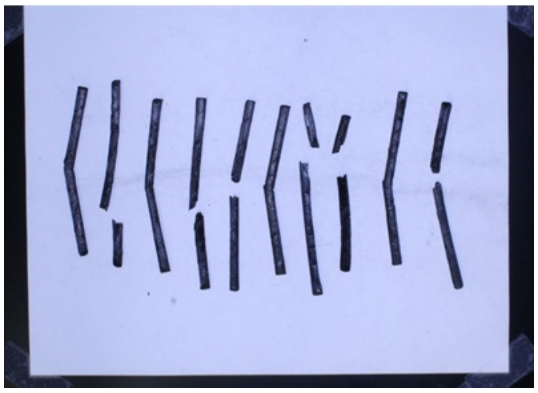

Figure 4.5: Photograph of poplar dowels of diameter 1/4 in (6.35 mm) with flaming exposure for 10 s after bending tests.

4.2 Comparison of Maximum Values between Heating Modes

In order to quantify the results from the physical observations discussed in Section 4.1, the maximum forces that each dowel could withstand prior to breakage were studied as a function of the initial diameter of the dowels for all the tests. Ten dowels were tested for each testing scenario for both the hot plate and flaming tests, and the mean of the maximum force for each testing condition was calculated to find the average value associated with the test parameters. Figures 4.6(a) and 4.6(b) show the average maximum force for birch dowels tested on the hot plate at a constant temperature of 350°C for increasing times and a constant time of 15 min with increasing temperatures, respectively.

Tables 4.1 and 4.2 present the equations that were used to fit the data points and the R^2 values associated with each. These results show that the maximum force decreases exponentially with decreasing diameters. A comparison of these figures shows that increasing the temperature had a larger effect on the value of

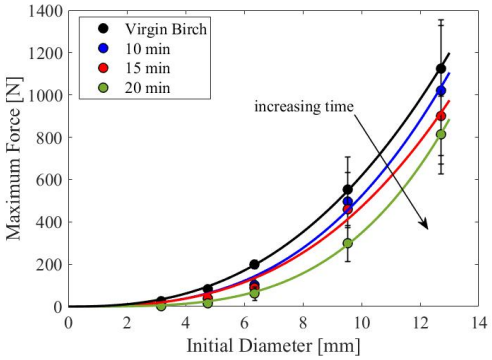

(a) Birch dowels on hot plate with increasing times.

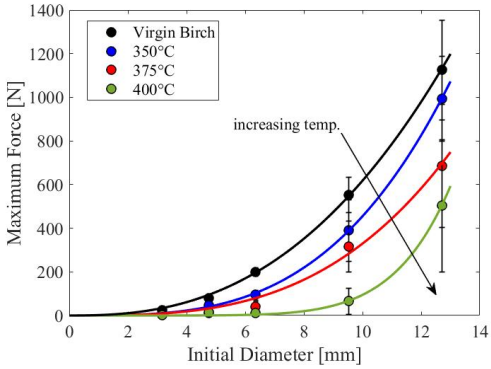

(b) Birch dowels on hot plate with increasing temperatures.

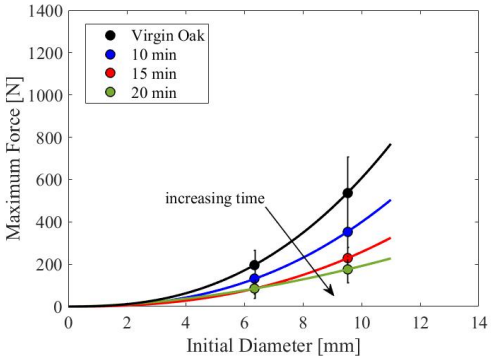

(c) Oak dowels on hot plate with increasing times.

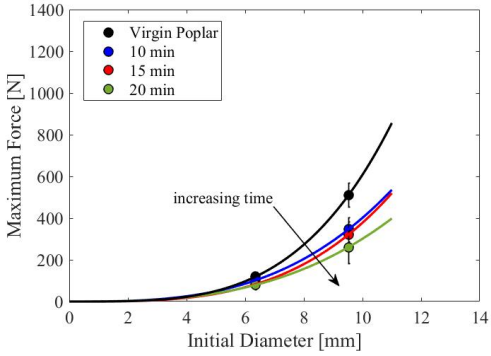

(d) Poplar dowels on hot plate with increasing times.

Figure 4.6: Comparison of maximum force as a function of initial diameter for all hot plate tests. The maximum force decreases as a function of time and temperaure. It can also be seen that temperature had a more significant effect than time, when comparing (a) and (b).

Table 4.1: The equations and R^2 values used to fit the data for birch dowels heated on the hot plate with *increasing exposure times*.

Wood Condition	$F_{max} = aD_0^b$ a	b	R^2
Virgin	1.85	2.53	1
10 min	0.724	2.86	0.99
15 min	0.804	2.77	0.99
20 min	0.094	3.57	1

Table 4.2: The equations and R^2 values used to fit the data for birch dowels heated on the hot plate with *increasing exposure temperatures*.

Wood Condition	$F_{max} = aD_0^b$ a	b	R^2
Virgin	1.84	2.53	1
350°C	0.244	3.27	1
375°C	0.245	3.13	0.99
400°C	9.38E-6	7.00	1

the maximum force compared to increasing the time, which supports the visual observations made in Section 4.1. The error bars in these figures represent the standard deviation from the average value for the respective testing condition, which each contained ten samples. The hot plate tests using oak and poplar are not as valuable because an accurate trend cannot be formed, since only two diameters were tested. However, the values for these tests were still plotted, but the equations of the fits and the R^2 values are not provided. These graphs were included, because they do illustrate that the exposure time had a larger effect on the maximum force for the oak dowels when compared to the poplar dowels, as shown in Figures 4.6(c)

and 4.6(d). It is also interesting to note that the mean maximum forces for the oak tests had a larger standard deviation when compared to the poplar tests.

The mean values of maximum force were also calculated for the flaming tests to observe the trends when burning time was increased for the multiple diameters tested. These results are shown in Figure 4.7 for all three species. In the birch tests, the maximum forces decreased with increasing time fore each diameter, as illustrated in Figure 4.7(a). The results of the oak tests, given in Figure 4.7(b), demonstrate that increasing the exposure time from 15 s to 20 s did not significantly change the maximum force measured for any of the sizes. The poplar dowels lost a lot of strength after burning for 10 s, but increasing the exposure time beyond 10 s only created small decreases in the ultimate force, which can be seen in Figure 4.7(c). These figures also demonstrated that the standard deviation increases with increasing diameter. The range of maximum forces for respective diameter size in the hot plate tests are similar to those measured from the flaming tests, which can be seen when Figure 4.6 is compared to Figure 4.7.

Table 4.3: The equations and R^2 values used to fit the data for **birch** dowels heated in the flame with increasing exposure times.

Wood Condition	$F_{max} = aD_0^b$ a	b	R^2
Virgin	1.76	2.54	1
10 min	0.286	3.23	0.99
15 min	0.053	3.83	0.99
20 min	0.012	4.29	0.99

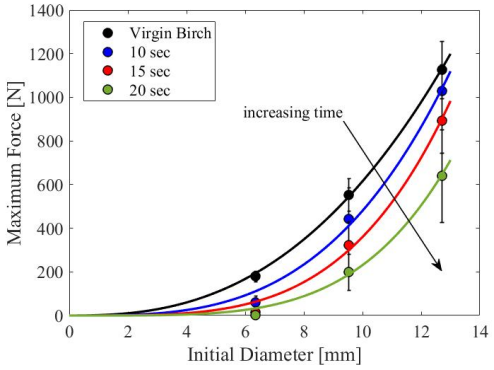

(a) **Birch** dowels from flaming tests with increasing times.

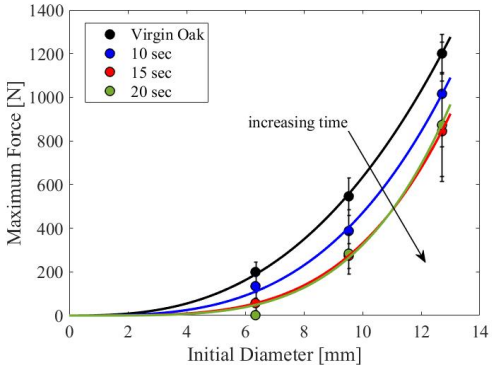

(b) **Oak** dowels from flaming tests with increasing temperatures.

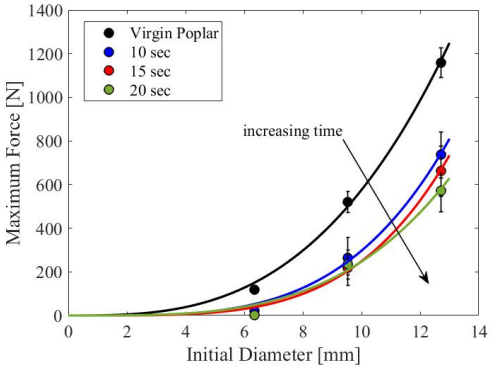

(c) **Poplar** dowels from flaming tests with increasing times.

Figure 4.7: Comparison of maximum force as a function of initial diameter for all flaming tests. The maximum force decreases as a function of time in all cases.

Table 4.4: The equations and R^2 values used to fit the data for **oak** dowels heated in the flame with increasing exposure times.

Wood Condition	$F_{max} = aD_0^b$ a	b	R^2
Virgin	1.35	2.67	1
10 min	0.293	3.21	1
15 min	0.040	3.92	1
20 min	0.021	4.17	0.99

Table 4.5: The equations and R^2 values used to fit the data for **poplar** dowels heated in the flame with increasing exposure times.

Wood Condition	$F_{max} = aD_0^b$ a	b	R^2
Virgin	0.641	2.95	1
10 s	0.045	3.82	0.99
15 s	0.019	4.13	0.99
20 s	0.067	3.56	0.98

Barr and Ezekoye [13] performed bending tests on cylindrical Yellow poplar dowels to determine strength characteristics after heating. They used dowels with three different initial diameters, 4.8 mm, 6.4 mm, and 7.9 mm, and each rod was 20 cm long. The experiments were divided into three testing scenarios: ambient 14°C, oven heating at 101°C for 1 hour, and oven heating at 250°C for 1 hour. From these experiments, Barr and Ezekoye [13] found a linear relationship between the flexural strength and density of the dowel. Table 4.6 gives the equations of the lines and R^2 values for their data.

A comparison between their findings and the results of the hot plate and

Table 4.6: Equations of the linear fits for data from [13] and their respective R^2 values.

Literature data [13]	$MOR = a\rho + b$ a	b	R^2
101°C for 1 hr	0.282	25.5	0.57
250°C for 1 hr	0.186	16.1	0.43

flaming tests is made to determine if a linear relationship is correct. Barr and Ezekoye [13] used the critical, or maximum, load for fracture in calculating the flexural strength. In other words, they studied the relationship between the MOR and the density of the dowel after heating. MOR can be calculated by converting the force measured to the axial stress, σ, induced on the dowel by using the following expression

$$\sigma = \frac{My}{I} \tag{4.1}$$

where M is the bending moment, y the distance from the neutral axis, and I the second moment of inertia. The maximum bending moment, M_{max}, is given by the maximum concentrated load, F_{max}, applied at the midspan, with length L_s in between supports, and is given by

$$M_{max} = \frac{F_{max} L_s}{4}. \tag{4.2}$$

The distance from the neutral axis, y, is equal to $D/2$, where D is the diameter of the dowel. Lastly, the second moment of inertia, I, of a cylindrical rod is

$$I = \frac{\pi D^4}{64}. \tag{4.3}$$

This is calculated using the initial dowel diameter, because there is relatively no change due to the short exposure times. Combining these expressions together

results in the formulation of the MOR produced during the three-point bending tests:

$$MOR = \frac{8F_{max}L_s}{\pi D^3}. \tag{4.4}$$

Due to the short exposure times in these experiments, the volume of the dowels is mostly unchanged after heating, so the final density, ρ_f, is calculated using

$$\rho_f = \frac{m_f}{V} \tag{4.5}$$

where m_f is the mass after heating and V the initial volume of the dowel. The volume used is the volume of a cylinder, which is given by

$$V = \frac{\pi D^2 L}{4}. \tag{4.6}$$

A plot with this data from all of the hot plate tests is shown in Figure 4.8. Included on each graph is the linear fit found by Barr and Ezekoye [13] for poplar dowels exposed to 250°C for 1 hr. The equations of the lines used to fit the hot plate data and associated R^2 values are given in Table 4.7. These figures show that there is a trend of decreasing MOR with decreasing density, and they give insight into the effect of species. The slopes of the fits change for the different species, so the how quickly the strength decreases due to density will vary dependent on species. Therefore, it is reasonable that the results of the poplar tests are closest with the fit from [13], because the dowels in these tests were also poplar.

Using the failure data from the flaming tests, however, suggests that the previous tests only explained part of the structure mechanics, as seen when comparing Figure 4.9 to Figure 4.8. When looking at a wider range of final densities, it becomes

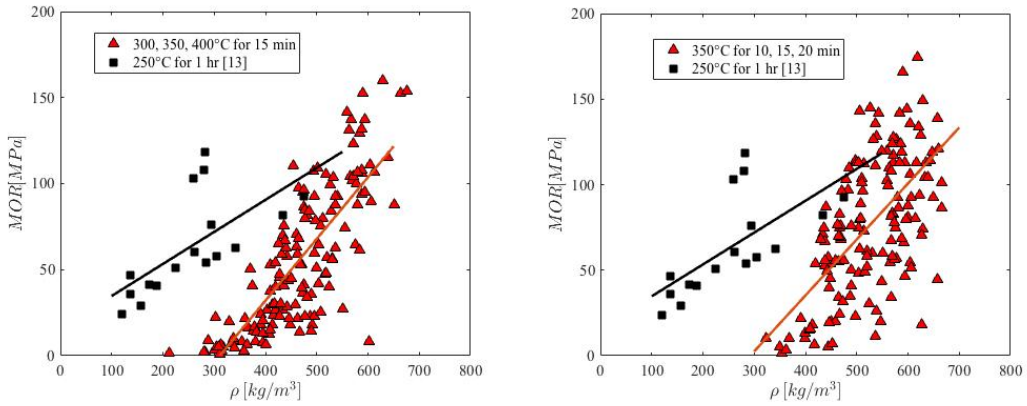

(a) Birch (constant temp.)

(b) Birch (constant time)

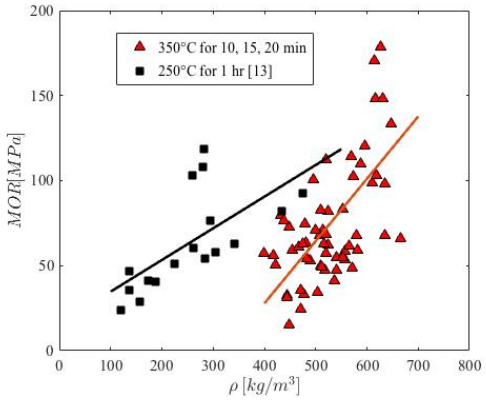

(c) Oak

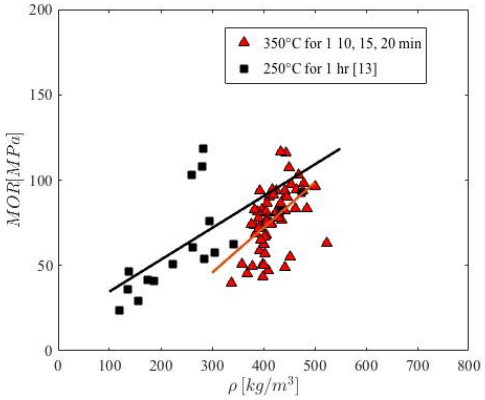

(d) Poplar

Figure 4.8: MOR as a function of density for various hot plate tests with a comparison to the fit from [13] for heating at 250°C.

Table 4.7: Summary of equations and R^2 values for the fits for the hot plate tests.

Test Conditions	$MOR = a\rho + b$ a	b	R^2
Birch, 350°C tests	0.327	-95.7	0.38
Oak, 350°C tests	0.366	-119	0.42
Poplar, 350°C tests	0.264	-33.4	0.26
Birch, 15 min tests	0.359	-112	0.64

clear that the relationship between MOR and density has two distinct regimes. The regime with higher densities was fitted with a linear line to make a comparison with the hot plate tests. By observing the equations for these lines, given in 4.8, it is clear that the species determines the slope of these lines. Any specimen with a final density below 300 kg/m^3 was more easily breakable, as signified by the very low values of MOR. Studying how the maximum stress, or MOR, changes with the final density of the specimen allows for a first connection between structural properties and combustion to be made, because the final density is dependent on initial properties and mass loss from combustion.

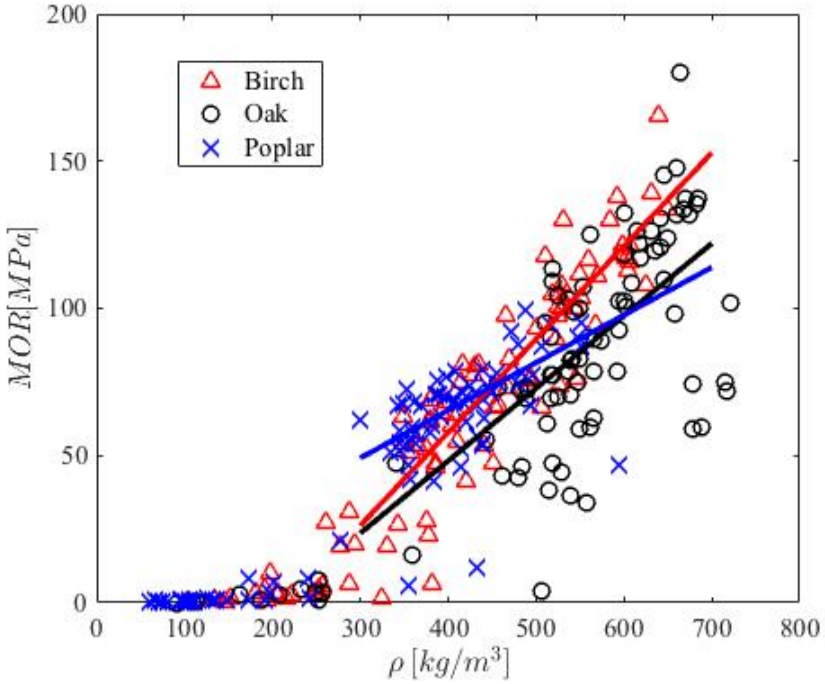

Figure 4.9: MOR as a function of density for data from all flaming tests. This shows the relationship between MOR and density has two regimes.

Table 4.8: Summary of the equations and R^2 values for the fits for second regime of the flaming tests.

Wood Species	$MOR = a\rho + b$ a	b	R^2
Birch	0.316	-68.8	.82
Oak	0.246	-50.2	0.34
Poplar	0.162	0.608	0.50

4.3 Breakage Mechanics for Flaming Tests

As mentioned earlier, the data for the flaming tests resulted in a more comprehensive analysis of the relationship between structural properties and combustion effects, so these results were studied in more detail. To gain a deeper understanding of the structural breakage process, stress and strain relationships are calculated for each bending test. The formulation for the stress applied to the dowel is the same as Equation 4.1, but the bending moment, M, is now given by

$$M = \frac{FL_s}{4} \tag{4.7}$$

where F is the applied force throughout the bending test, not just the maximum, and L_s still the length span between supports. This results in the final expression for applied stress, σ, throughout the duration of a test to be

$$\sigma = \frac{8FL_s}{\pi D^3}. \tag{4.8}$$

Using Hooke's Law, $\sigma = E\epsilon$, where E is the modulus of elasticity and ϵ the strain, and Equation 4.1, the strain can be written as

$$\epsilon = \frac{My}{EI}. \tag{4.9}$$

In order to calculate the strain applied in the experiments, the modulus of elasticity must be removed from Equation 4.9 by dividing it by the deflection of the dowel, δ. In a simply supported beam with a concentrated load, F, applied at the center, the deflection is defined by

$$\delta = \frac{FL_s^3}{48EI}. \tag{4.10}$$

Dividing the definition of strain, Equation 4.9, by the deflection will eliminate the modulus of elasticity and give the final expression for calculating strain:

$$\epsilon = \frac{6D\delta}{L_s^2}. \tag{4.11}$$

The deflection is a quantity that is directly measured during the tests by the position of the plunger as soon as it is applied to the dowel. It is important to note that the expression for strain is only truly valid for elastic behavior, since it was formulated using Hooke's Law.

Using Equations 4.8 and 4.11, stress-strain curves can be formulated for each test. Each exposure time had an equal number of dowels tested for each species, so the stress-strain relationship for each group of tests was averaged. Mean stress-strain relationships were first calculated for the three diameter sizes of the birch, oak, and poplar dowels, so that it is clear how the combustion process effects the bending process. The modulus of elasticity, E, can be calculated for each case by finding the slope of the linear portion of the stress-strain curve, as given by Hooke's Law. Both the diameter and the species of wood effected the shape of the stress-strain curve and the value of modulus of elasticity, even for the virgin wood, as shown in Figure 4.10. Note that the stress-strain curves for the oak and poplar are not extended

Table 4.9: Literature data for E and MOR from [9].

	Birch, Paper	**Oak, Northern Red**	**Poplar, Yellow**
E (MPa)	11,000	12,500	10,900
MOR (kPa)	85,000	99,000	70,000

as long as the birch, because these tests were stopped sooner. This is because the elastic region of the curve is the region of interest, not the plastic region.

A mean value of modulus of elasticity was calculated from the stress-strain relationship for the tests of the virgin wood by calculating the slope of the linear portion of the graph, and a mean value of MOR was found as the maximum stress on the stress-strain curves. Table 4.10 gives the calculated values of E and MOR for the virgin wood. The experimental results illustrate that the modulus of elasticity decreases with increasing size diameters for all three species. This behavior was unexpected, as E usually does not have a dependence on material size. After a review of the literature in reference to this behavior, it was discovered that nano-sized materials saw an increased in modulus of elasticity with decreasing diameters [42,43]. The dowels used in these experiments are not on the nano-scale, so this behavior should be further studied in the future. It can be observed that the MOR also decreased with increasing diameter for the birch and oak dowels, which is expected behavior and is in agreeance with the statistical strength theory, discussed in Section 2.2. This was not true for the poplar dowels, though. Literature data of these properties from [9] is presented in Table 4.9 for Paper Birch, Northern Red Oak, and Yellow Poplar, all with a 12% moisture content. The experimental measurements

Table 4.10: Overview of the calculated values for E and MOR for virgin wood of each species and diameter.

	Birch		**Oak**		**Poplar**	
D (mm)	E (MPa)	MOR (kPa)	E (MPa)	MOR (kPa)	E (MPa)	MOR (kPa)
6.35	9,300	150,090	11,260	162,310	6,385	91,237
9.525	6,102	127,470	6,369	130,130	5,642	127,490
12.7	3,502	107,420	4,093	121,270	3,632	118,870

and the literature data do not match exactly, but it is clear from both sets of values that oak is the strongest and poplar is the weakest.

Table 4.11: Calculated MOR values for all three species and diameters for the various exposure times.

	Birch			**Oak**			**Poplar**		
	MOR (kPa)			MOR (kPa)			MOR (kPa)		
D(mm)	10 s	15 s	20 s	10 s	15 s	20 s	10 s	15 s	20 s
6.35	46,356	10,351	2,797	110,830	44,654	2,271	22,119	2,480	-
9.525	104,650	76,071	45,239	92,205	63,459	60,847	60,901	53,338	58,695
12.7	101,480	86,697	64,530	99,699	79,390	80,393	72,684	67,709	55,340

Figures 4.11 - 4.13 give the stress-strain curves for the birch, oak, and poplar, respectively. The effect of the flaming times can be seen for each diameter size. In the flaming tests, the MOR was found to increase with increasing size for each respective exposure time, as shown in Table 4.11. The MOR of the virgin wood, however, decreased with increasing size. This shows the degradation and weakening effects of combustion. It was found that flaming times of only 20 s could produce at least a 33% loss of strength for the 12.7 mm (1/2 in) diameter dowels and at least a 53% loss for 9.525 mm (3/8 in) dowels. The 6.35 mm (1/4 in) diameter

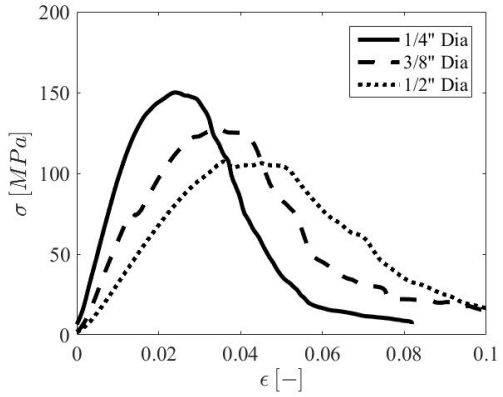

(a) Virgin Birch

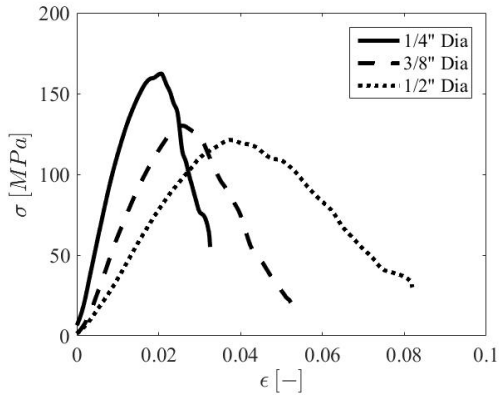

(b) Virgin Oak

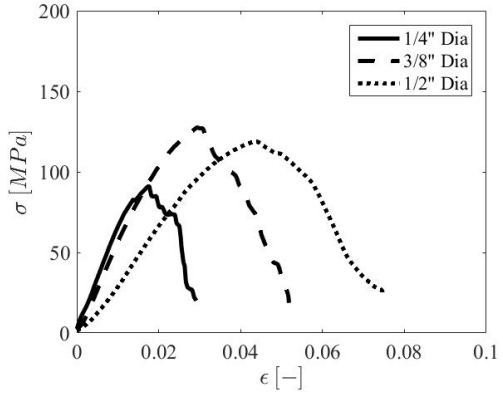

(c) Virgin Poplar

Figure 4.10: Stress-strain curves for the virgin wood.

dowels resulted in about a 90% strength reduction for a 20 s exposure. It is also noted that the smaller diameter dowels reached their respective MOR values at lower values of ϵ compared to the larger diameters. The standard deviation of these curves increases with larger diameters, where the 12.7 mm (1/2 in) diameter have a standard deviation of about 35 MPa from the mean, the 9.525 mm (3/8 in) dowels have a standard deviation of about 20 MPa, and the 6.35 mm (1/4 in) diameter dowels have a standard deviation of about 6 MPa for all three species.

The types of vegetative fuels modeled in this study often have branching geometries. These geometries have the potential to effect the breakage mechanics; however, these measurements are still valuable to studying firebrand generation. Barr and Ezekoye [13] performed similar tests, as discussed above, to study the effect of oven heating on the strength of dowels and used a fractal model to represent the branching geometry. Combining their results on dowel strength and a fractal model, they were able to create a relationship that extended the three-point bending tests to a branching configuration.

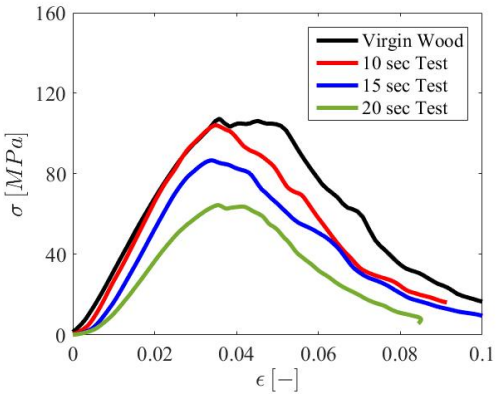

(a) 12.7 mm (1/2 in) diameter Birch

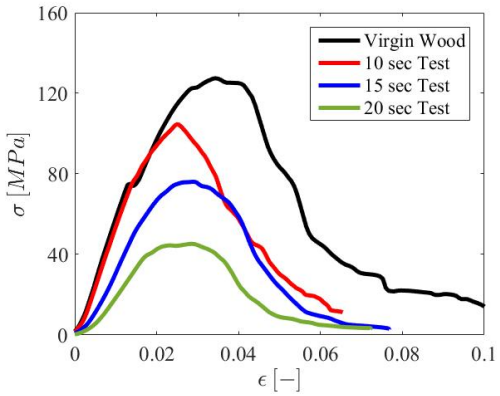

(b) 9.525 mm (3/8 in) diameter Birch

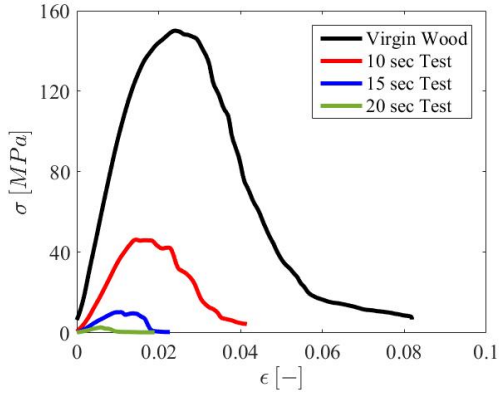

(c) 6.35 mm (1/4 in) diameter Birch

Figure 4.11: Stress-strain curves for the three diameters of birch.

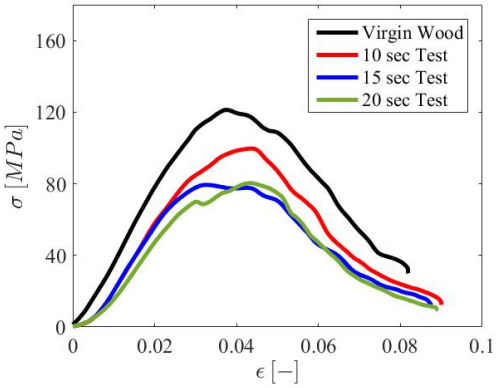

(a) 12.7 mm (1/2 in) diameter Oak

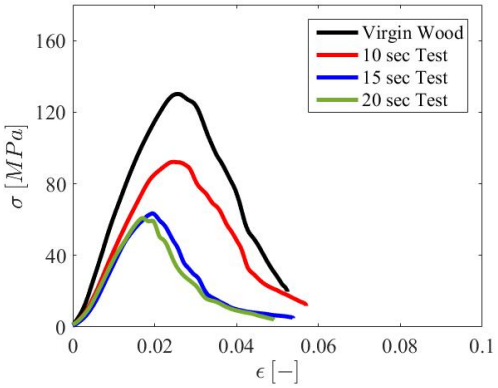

(b) 9.525 mm (3/8 in) diameter Oak

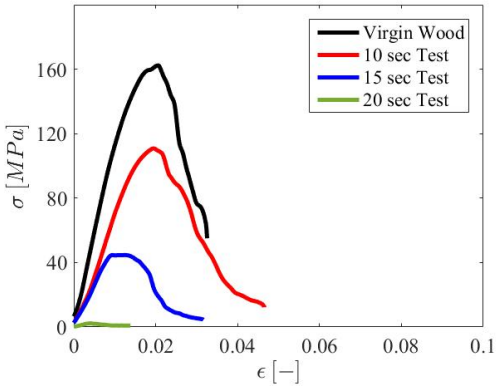

(c) 6.35 mm (1/4 in) diameter Oak

Figure 4.12: Stress-strain curves for the three diameters of oak.

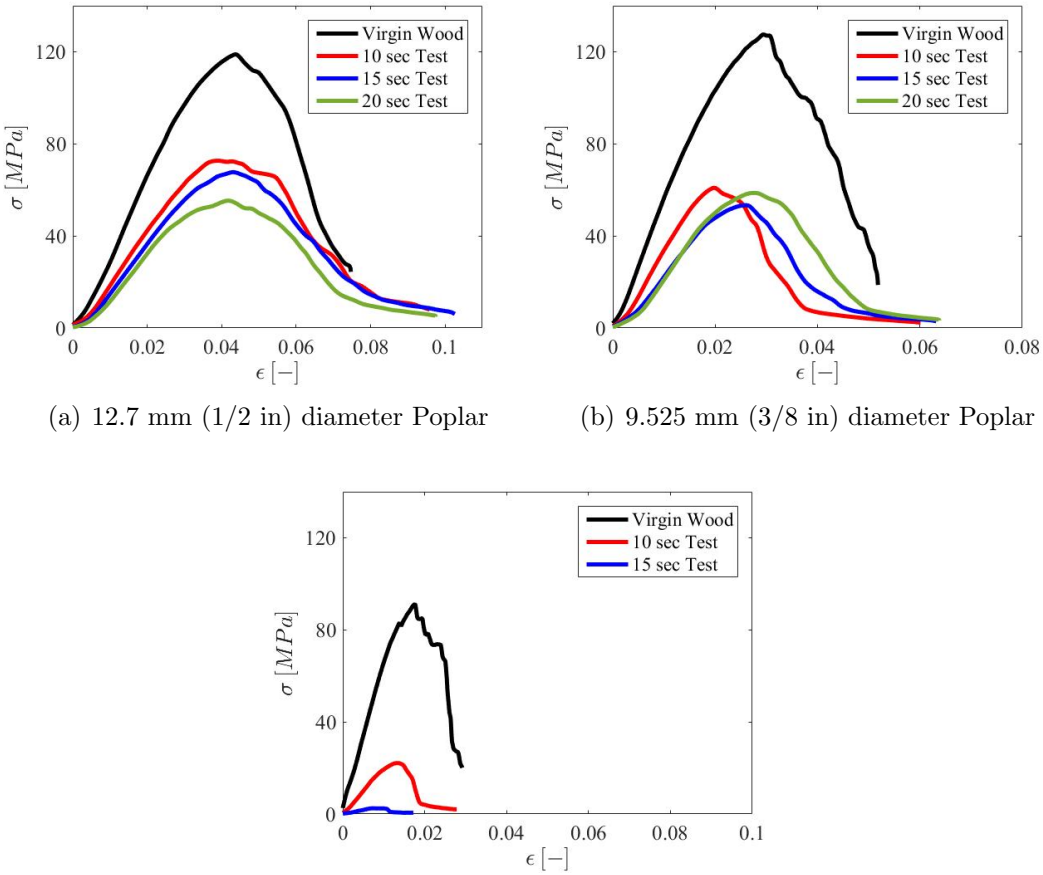

(a) 12.7 mm (1/2 in) diameter Poplar

(b) 9.525 mm (3/8 in) diameter Poplar

(c) 6.35 mm (1/4 in) diameter Poplar

Figure 4.13: Stress-strain curves for the three diameters of poplar. Note that the results for 6.35 mm (1/4 in) dowels were too small to be plotted.

Chapter 5: Analysis

5.1 Non-dimensional Scaling for Flaming Tests

The results of the three-point bending tests produced valuable knowledge on how combustion processes affect the strength and breakage mechanics of cylindrical wooden dowels. The results, however, are specific to the species and sizes being tested, so it is beneficial to use non-dimensional scaling to find a more universal relationship to describe the breakage phenomena of firebrands. The critical, or maximum, breakage force should be scaled by using the controlled variables and the measured parameters from the experiments and by incorporating structural and combustion properties to form a model of the important parameters. This can be shown by combining the controlling parameters in the following relationship:

$$F_{max} = f(\rho_0, L_0, D_0, \nu, \alpha, \dot{m}, E, \rho_\infty), \tag{5.1}$$

where F_{max} is the critical force for breakage, ρ_0 the initial species density, L_0 the initial length of the dowel, D_0 the initial dowel diameter, ν Poisson's ratio, α species thermal diffusivity, $\dot{m}$ the mass loss rate, E the modulus of elasticity, and ρ_∞ the denisty of the air. These controlling parameters can be fit into four separate categories. L_0 and D_0 strictly describe the geometry of the dowel; these two parameters can be grouped with ρ_0 to describe the initial conditions and characteristics of the

dowel. Including ν and E is important because these parameters define the fracture mechanics. $\dot{m}$ and ρ_∞ can be grouped together to describe the burning, and α is a description of thermal properties. At first, it was not clear if the thermal properties had a direct role in this process, but when α was included in the parameter list, it helped to collapse the data. This simple model is developed to first understand how these values, which were measured or known material constants, interact before creating a more generalized and detailed model that incorporates the added effects of wind.

This scaling analysis is based on the Buckingham Pi theorem, which allows for nondimensional parameters to be created through the method of repeating variables. For this simplified scaling, there are a total of nine parameters, which are shown in Equation 5.1, and the three primary dimensions present are mass (M), length (L), and time (T). The reduction is defined as the number of primary dimensions and governs the number of repeating variables needed; therefore, three repeating variables are chosen such that they cover the entire dimension space. The scaling can now be re-written to illustrate the chosen repeating variables as

$$F_{max} = f(L_0, \nu, \alpha, \dot{m}, \rho_\infty | D_0^a \rho_0^b E^c). \tag{5.2}$$

This formulation reveals six nondimensional Π groups, which are

$$\Pi_1 = \frac{F_{max}}{E D_0^2}, \quad \Pi_2 = \frac{L_0}{D_0}, \quad \Pi_3 = \nu, \quad \Pi_4 = \frac{\alpha^2 \rho_0}{E D_0^2}, \quad \Pi_5 = \frac{\dot{m}}{D_0^2 \sqrt{\rho_0 E}}, \quad \Pi_6 = \frac{\rho_\infty}{\rho_0} \tag{5.3}$$

Π_1 is a ratio of the force needed for fracture over the resistance to deformation. Π_2 is a nondimensional description of the geometry; this term is often given the name

η, as seen in [40]. Π_3, ν, is the ratio of transverse strain to axial strain, and Π_6 is the ratio of air density to species density. Π_4 and Π_5 are not as straightforward as the other Π groups. Π_4 can be thought of as a thermal capacity over a resistance to deformation, and Π_5 is thought of as a nondimensional burning rate.

The Buckingham Pi theorem is useful because it gives a relationship between Π groups as

$$\Pi_1 = f(\Pi_2, \Pi_3, ..., \Pi_n). \tag{5.4}$$

This allows for manipulation of the calculated Π groups to form two main nondimensional parameters that are meaningful and descriptive of the problem that needs to be modeled. The two final nondimensional parameters used in this firebrand breakage model are

$$\Pi_1^* = \frac{F_{max} L_0 \nu}{E D_0^3}, \qquad \Pi_2^* = \frac{\dot{m} \alpha \rho_0}{E D_0^3 \rho_\infty}. \tag{5.5}$$

Multiplication of Π_1, Π_2, and Π_3 results in Π_1^*, which is a nondimensional formulation of the transverse strain due to bending. This is seen by defining

$$\sigma = \frac{FL}{D^3}, \tag{5.6}$$

$$E = \frac{\sigma}{\epsilon_{axial}}, \tag{5.7}$$

$$\nu = \frac{\epsilon_{trans}}{\epsilon_{axial}}, \tag{5.8}$$

where ϵ_{trans} and ϵ_{axial} are transverse and axial strain, respectively. If ν is removed from Π_1^*, this parameter is converted to the axial strain in bending. Π_2^* is created by multiplying the square root of Π_4 by Π_5 and then dividing by Π_6. For this analysis, Π_2^* is defined as ratio of the capacity for the material to burn over the capacity of the material to fail.

Data from the bending tests performed on the dowels that were exposed to flaming conditions was used to calculate Π_1^* and Π_2^*. L_0 and D_0 are controlled variables that are specific to the geometry of the tested dowels. Poisson's ratio, ν, and thermal diffusivity, α, are material properties dependent on species. The values used for ν were 0.426, 0.35, and 0.318 for birch, oak, and polar, respectively. These values were reported in [9] for yellow birch, red oak, and yellow poplar that were approximately at 12% moisture content. The thermal conductivity for wood is relatively low compared to other materials, like brick and metal. A typical value for wood is approximately 1.6 x 10^7 m^2/s [9], which is what was used in this analysis. The density of the air was taken to be a constant value of 1.2 kg/m^3. Although E was measured for each test condition, the values of E given in Table 4.9 were used in the analysis. E is defined as a material property, so it would be best to use the a priori value in the literature, rather than the calculated values from the experiments. The measured values of F_{max}, $\dot{m}$, and ρ_0 were all used in the calculations of Π_1^* and Π_2^*. Values for the two Π groups were calculated and plotted on a loglog scale to display the range of data collected, which is shown in Figure 5.1.

As indicated previously in Figure 4.9, Figure 5.1 illustrates that there are two distinct regimes in these experiments. There is one regime, shown by the horizontal green line, that is controlled by the burning rate parameter, Π_2^*, and a second regime, shown by the vertical yellow line, that is the controlled by Π_1^*, the nondimensional strain. The strain induced by the maximum force is constant until a critical value of about 2.2 x 10^{-12} is achieved by the burning rate parameter. At this value, the critical breakage forces drop off significantly, indicating that this regime is more

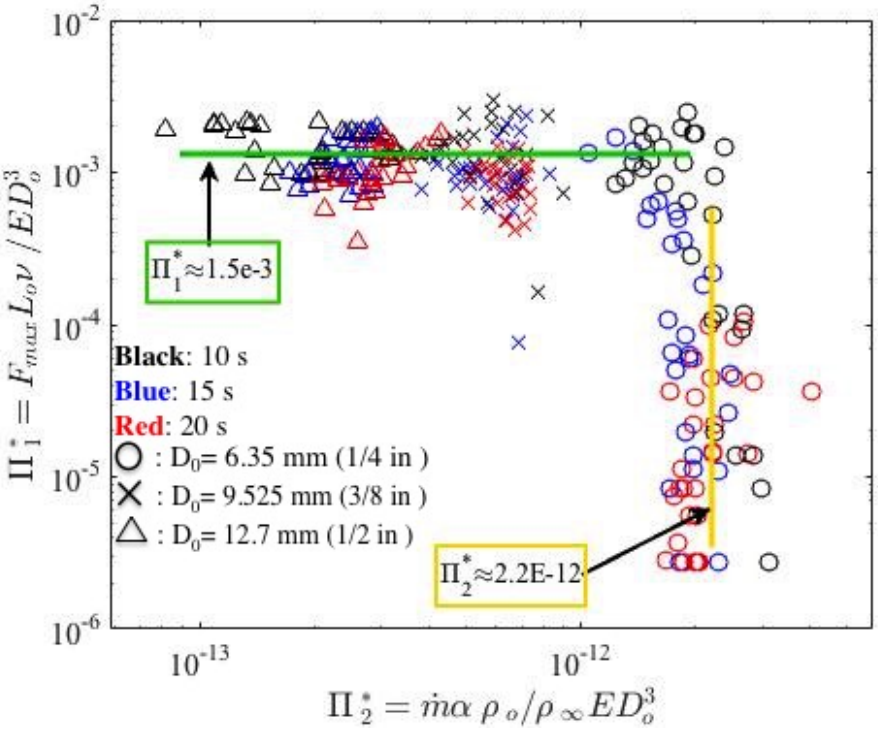

Figure 5.1: Nondimensional scaling of parameters in flaming tests that measure the degradation of dowel material properties due to heating.

easily susceptible to breakage. The mass-loss rate and thermal diffusivity are assumed to be two important parameters controlling this transition. The mass-loss rate incorporates the time of heating, which is necessary to get more information on the breakage process. The time provides an indication of how long heating is needed to degrade the vegetation and result in breakage, which gives an insight into when burning branches in WUI fires will break. Heating time and geometry characteristics would be information needed inputs for modeling firebrand generation.

It is also clear from Figure 5.1 that the diameter size is another factor that controls the transition. The 6.35 mm (1/4 in) diameter dowels, shown by the open circles, are all in the regime that is dominated by Π_1^* meaning that they fractured

the easiest and are not dependent on $\dot{m}$ because of their size. The flaming time, shown by the changing colors, also shows an intuitive trend. For the 12.7 mm (1/2 in) diameter dowels the Π_2^* values increase with increasing flaming times, which makes sense as $\dot{m}$ is a controlling parameter in this regime. A trend dependent on exposure time can also be seen in the other regime demonstrating that the dowels were more susceptible to fracture after longer amounts of time. The species are not distinguished in Figure 5.1 because there was no trend specific to the species, which means that these relationships and regimes should be valid for all species.

5.2 Incorporating Wind Effects

All of the results and analysis thus far have been focused on strength and breakage properties of wood based solely on the effects of degradation due to combustion. The effects of degradation and wind, however, must be studied in conjunction to create a comprehensive firebrand breakage model. Wind has a critical role in the process of firebrand generation for two main reasons. The first is that it imposes drag forces on the burning vegetation, which have the ability to cause fracture. It also has the potential to alter the burning rate, which will influence the degradation process. Consequently, it is necessary to study the coupling effect of the wind and degradation to fully understand the details of firebrand production.

An estimation of the wind speeds needed to cause the critical forces measured in the three-point bending experiments can be made by using the correlation between drag coefficient and Reynolds number and the simplified breakage model given by [40] in Equation 2.5, which was described earlier.

For this discussion, Equation 2.5 is simplified to

$$MOR = \sqrt{\left(\frac{8\rho_\infty C_D U_h^2 \eta^2}{\pi}\right)^2 + (4\rho_0 g L \eta)^2}. \tag{5.9}$$

The term that included the effect of the vertical drag forces is neglected for this analysis, so that an estimation of the horizontal wind speeds needed to cause the MOR can be found. This equation can be re-written to solve for the horizontal wind velocity, U_h, as

$$U_h = \left[\frac{\sqrt{\pi^2 \left(MOR^2 - (4\rho_0 g L \eta)^2\right)}}{8\rho_\infty C_D \eta^2}\right]^{1/2}. \tag{5.10}$$

This equation relates the horizontal wind velocity to the MOR and stresses caused by the weight of the dowel. The weight is included because in real WUI scenarios branches are not simply supported, instead they resemble a cantilever beam, and the force from the weight creates a moment. Everything in Equation 5.10 is known except for the drag coefficient, C_D. To solve for the wind velocity, an initial guess of this value is made so that the Reynolds number can be calculated. A value for C_D corresponding to this Reynolds number is found from the relationship of C_D and Re over a smooth cylinder. This value for C_D is used in Equation 5.10 to calculate U_h. This process was iterated until the velocity guess is within 0.001 m/s of the calculated U_h.

This calculation was performed for the three species, but only used the data from tests with a flaming time of 20 s. In reality, vegetation will have much longer exposure times than this, so the two lower flaming times are not considered. Figure 5.2 shows the results of this analysis. The length of the dowel was increased in increments of 5 cm starting from 10 cm, which was the length of the dowels tested.

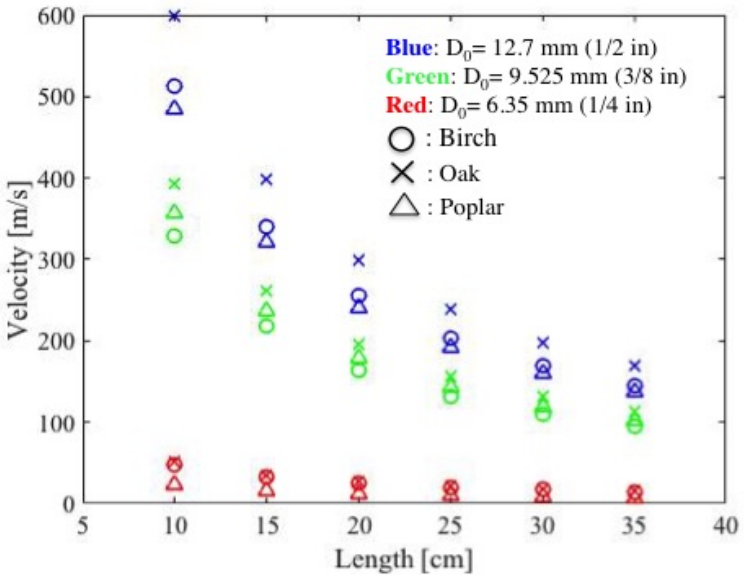

Figure 5.2: Wind speeds predicted by Equation 5.10 as a function of dowel length.

As expected, decreasing the diameter also decreases the wind speed. Increasing the length of the dowel increases the drag force, so the wind speed needed for fracture will decrease. It can also be seen that the species plays a small role in determining the critical winds speeds. The wind speeds predicted for the 6.35 mm (1/4 in) diameter are reasonable velocities to occur during WUI fire, approximately 15 m/s. The larger diameters, however, predicted unrealistic values needed for breakage. This is an indication that these sizes do not fracture until they degrade down to a critical size.

Manzello et al. [28,29] found that firebrands collected from experimental burns of Douglas fir and Korean pine trees had average diameters between 3 mm and 5 mm. There was no applied wind in these tests, so the firebrands collected in these tests fractured only due to degradation. A study of firebrand sizes from the Bastrop Complex fire reported that the majority of firebrands had a projected area

of 0.5 cm^2, and during this fire, winds were recorded to range from 5 m/s to 6 m/s with gusts reaching 14 m/s [38]. Houssami et al. [39] performed a field study that found branches on a shrub less than 2 mm in diameter were no longer attached and branches between 2 mm and 4 mm diameter were partially consumed after the fire passed. The winds during this fire were similar to the ones reported for the Bastrop Complex fire.

The Beaufort Wind Scale and the Fujita Scale, discussed previously, indicate that wind speeds between 17 m/s and 32 m/s have the ability to break branches off of trees, which agrees with the range of wind speeds predicted to cause fracture for the 6.35 mm (1/4 in) diameter dowels. A study conducted by Virot et al. [44] examined critical wind speeds needs to breakage trees during storms with high winds. Their model showed that the critical wind speed for trunk breakage was weakly dependent on tree size (height and trunk diameter), which is inconsistent with the predictions made in this thesis. This suggest that the breakage mechanisms for branches is different than the breakage mechanisms for tree trunks. They also found that the difference between critical wind speeds between hardwoods and softwoods was less than 10% from their model, which was in compatible with a storm that occurred in France that they used for comparison. This finding provides confidence that the results presented here for hardwoods can also predict critical wind speeds for softwoods, which are typically found in WUI areas.

There is little degradation of firebrands while they are in transport because smoldering combustion is slow, so the sizes of the collected firebrands are a good estimation of the size at breakage. The results from the previous studies demonstrate

that the majority of firebrands produced from burning vegetation are small. The 6.35 mm (1/4 in) diameter dowels tested in the current study are slightly outside of the range of the typical size collected. However, the wind speeds reported in the previous work are lower than what was predicted to be necessary to cause breakage for the 6.35 mm (1/4 in) diameter dowel. The model discussed above suggests that a branch with a diameter of 6.35 mm (1/4 in) and length of 30 cm (11.8 in) would fracture with applied winds of about 15 m/s. Since the studies reported gusts up to 14 m/s, some of the larger firebrands that were collected could have been produced during the times of gusting winds. The previous studies also suggest that these small firebrands are the ones that are lofted and carried downstream. The larger brands, while the may break due to their weight, are more likely to just fall to the ground at the lower winds speeds. It is evident that wind is a determining factor of the size of firebrands produced and a connection can be made between the role of degradation and wind in the firebrand generation process.

Chapter 6: Conclusion

This work developed a repeatable method for testing the effects of combustion on the strength of small cylindrical wooden dowels. After different heating modes were tested, it was found that using a flame created the most realistic conditions and produced a larger range of results. This was beneficial because similar work in the literature was missing this aspect. Three-point bending tests provided an efficient method for gaining knowledge on multiple aspects of the failure mechanics. The maximum applied load, stress, strain, modulus of elasticity, and modulus of rupture were calculated for birch, oak, and poplar dowels with diameters of 6.35 mm, 9.525 mm, and 12.7 mm (1/4 in, 3/8 in, 1/2 in, respectively) to determine the effect of species and size.

It was found that there were two main mechanisms for failure. This could be abrupt, complete failure or fibrous, splintering failure. The 6.35 mm (1/4 in) diameter dowels were the only ones to experience abrupt failure when using the exposed to the flames; however, larger sizes experienced this type of failure in other heating methods. This suggests that the combustion process is another controlling parameter of the fracture mechanics. If the flaming times were increased in these tests, the larger sizes could have experienced abrupt failure.

For all the species, it was found that the breakage is controlled by two distinct

regimes. The density is one of the parameters that controls these regimes. If the density is below 300 kg/m^3, the MOR is very small indicating that the stress needed for breakage is small. Above this value, there is a somewhat linear relationship where MOR increases with increasing density, but the species appears to control the rate of increase. All species saw a similar trend where the effect of the heating time was dependent on the size of the dowel. The smallest diameter was always most effected by the heating time, and the MOR decreased with increasing heating time, both of which were expected.

Predictions of the wind speeds associated with the critical stresses measured were calculated, because the connection between how heating and wind effects breakage is vital. These predictions suggested that the 9.525 mm and 12.7 mm (3/8 in and 1/2 in, respectively) diameters would not break from the heating exposure in these experiments, because the wind speeds predicted were not realistic. The wind velocities predicted for the 6.35 mm (1/4 in) diameter dowels are more reasonable, in comparison, even with the short exposure times. The dowels tested were shorter than most branches, so the length was increased to show the effect of increasing drag. The theory provides that increasing the length of the dowel results in wind speeds that could be experienced in WUI fire events for the 6.35 mm (1/4 in) diameter dowels.

There still needs to be an effort to further understand the connection between wind and combustion. Small-scale experiments that study the breakage of dowels in a wind tunnel is needed to determine the critical wind velocity and exposure time that results in breakage. These small-scale wind tunnel experiments will allow

for close examination and visual observation of the breakage process under real conditions. Direction of the wind needs to be considered, because the wind could be in the vertical direction representing buoyancy or the horizontal direction. This can be combined with the knowledge developed in this thesis on the effect combustion and thermal properties has on the fracture mechanics to develop a comprehensive model of firebrand generation.

Experiments involving real WUI fuels should also be included in future work to ensure that the relationships developed in this work scale in the same manner to all fuels. Branching geometries should also be considered, because the connections between branches can affect the breakage and needs to be studied. Combining these effects on the breakage mechanics and developing an accurate, comprehensive firebrand generation model will allow for better computational modeling of the spread of WUI fires by firebrands. It could also help to determine if certain areas are at a higher risk of firebrand attack depending on the surrounding fuel and fire conditions. Although more work on the effect of the wind is still needed, this work is the first step in understanding the controlling parameters governing firebrand production.

Bibliography

[1] Sara E Caton, Raquel SP Hakes, Daniel J Gorham, Aixi Zhou, and Michael J Gollner. Review of pathways for building fire spread in the wildland urban interface part 1: exposure conditions. *Fire Technology*, pages 1–45, 2016.

[2] John R Hall. The total cost of fire in the united states. 2014.

[3] AM Grishin, AI Filkov, EL Loboda, VV Reyno, AV Kozlov, VT Kuznetsov, DP Kasymov, SM Andreyuk, AI Ivanov, and ND Stolyarchuk. A field experiment on grass fire effects on wooden constructions and peat layer ignition. *International journal of wildland fire*, 23(3):445–449, 2014.

[4] Jack D Cohen. Preventing disaster: home ignitability in the wildland-urban interface. *Journal of forestry*, 98(3):15–21, 2000.

[5] Jack D Cohen and Richard D Stratton. Home destruction examination: Grass valley fire, lake arrowhead, california. 2008.

[6] Alexander Maranghides and William E Mell. *A case study of a community affected by the Witch and Guejito Fires*. National Institute of Standards and Technology. Building and Fire Research Laboratory, 2009.

[7] Samuel L Manzello. Enabling the investigation of structure vulnerabilities to wind-driven firebrand showers in wildland-urban interface (wui) fires. *Fire Safety Science*, 11:83–96, 2014.

[8] Michael A Ritter. *Timber bridges: design, construction, inspection, and maintenance*. Untied States Department of Agriculture, 1990.

[9] Robert J Ross et al. Wood handbook: Wood as an engineering material. 2010.

[10] Andrew Hamilton Buchanan. *Structural design for fire safety*, volume 273. Wiley New York, 2001.

[11] Samuel James Record. *The mechanical properties of wood, including a discussion of the factors affecting the mechanical properties, and methods of timber testing*. J. Wiley & sons, inc., 1914.

[12] A Van Casteren, WI Sellers, SKS Thorpe, S Coward, RH Crompton, and AR Ennos. Why dont branches snap? the mechanics of bending failure in three temperate angiosperm trees. *Trees*, 26(3):789–797, 2012.

[13] BW Barr and OA Ezekoye. Thermo-mechanical modeling of firebrand breakage on a fractal tree. *Proceedings of the Combustion Institute*, 34(2):2649–2656, 2013.

[14] Alexander Maranghides and Derek McNamara. *2011 Wildland Urban Interface Amarillo Fires Report# 2: Assessment of Fire Behavior and WUI Measurement Science*. National Institute of Standards and Technology. Engineering Laboratory, 2016.

[15] W Chaney. How wind effects trees. *Woodland Steward*, 10:1–8, 2001.

[16] Christopher J Luley, Andrew Plenïnger, and Susan Sisinni. The effect of wind gusts on branch failures in the city of rochester, new york, us. In *Tree Structure and Mechanics Conference Proceedings: How Trees Stand Up and Fall Down: October 2001, Savannah, Georgia, US*, page 103. International Society of Arboriculture, 2002.

[17] Frederick Lincoln Browne. Theories of the combustion of wood and its control. 1958.

[18] Esko Mikkola. Charring of wood based materials. *Fire Safety Science*, 3:547–556, 1991.

[19] Guillermo Rein. *Smoldering Combustion*, pages 581–603. Springer New York, New York, NY, 2016.

[20] Robert H White and Hao C Tran. Charring rate of wood exposed to a constant heat flux. 1996.

[21] Arijit Sinha, Rakesh Gupta, and John A Nairn. Thermal degradation of bending properties of structural wood and wood-based composites. *Holzforschung*, 65(2):221–229, 2011.

[22] Robert H White. *Charring rates of different wood species*. PhD thesis, University of Wisconsin-Madison, WI, 1988.

[23] Robert H White and Erik V Nordheim. Charring rate of wood for astm e 119 exposure. *Fire Technology*, 28(1):5–30, 1992.

[24] Bradford K Douglas. Calculating the fire resistance of exposed wood members. *American Forest & Paper Association. Washington DC, USA*, 2005.

[25] Robert H White. *Fire resistance of structural composite lumber products*. Unite States Department of Agriculture, Forest Service, Forest Products Laboratory, 2006.

[26] David W Green and James W Evans. The immediate effect of temperature on the modulus of elasticity of green and dry lumber 1. *Wood and Fiber Science*, 40(3):374–383, 2008.

[27] David W Green and James W Evans. Effect of cyclic long-term temperature exposure on the bending strength of lumber. *Wood and Fiber Science*, 40(2):288–300, 2008.

[28] Samuel L Manzello, Alexander Maranghides, and William E Mell. Firebrand generation from burning vegetation. *International Journal of Wildland Fire*, 16(4):458–462, 2007.

[29] Samuel L Manzello, Alexander Maranghides, John R Shields, William E Mell, Yoshihiko Hayashi, and Daisaku Nii. Mass and size distribution of firebrands generated from burning korean pine (pinus koraiensis) trees. *Fire and Materials*, 33(1):21–31, 2009.

[30] Thomas E Waterman. Experimental study of firebrand generation. Technical report, Illinois Institute of Technology, 1969.

[31] Frank J Vodvarka. *Firebrand Field Studies-Final Report*. Illinois Institute of Technology, 1969.

[32] Frank J Vodvarka. *Urban Field Burns-Full Scale Studies-Final Report*. Illinois Institute of Technology, 1969.

[33] Sayaka Suzuki, Samuel L Manzello, Matthew Lage, and George Laing. Firebrand generation data obtained from a full-scale structure burn. *International journal of wildland fire*, 21(8):961–968, 2012.

[34] Sayaka Suzuki, Adam Brown, Samuel L Manzello, Junichi Suzuki, and Yoshihiko Hayashi. Firebrands generated from a full-scale structure burning under well-controlled laboratory conditions. *Fire Safety Journal*, 63:43–51, 2014.

[35] Samuel L Manzello and Ethan ID Foote. Characterizing firebrand exposure from wildland–urban interface (wui) fires: results from the 2007 angora fire. *Fire Technology*, 50(1):105–124, 2014.

[36] Ethan ID Foote, John Liu, and Samuel L Manzello. Characterizing firebrand exposure during wildland urban interface fires. In *Proceedings of Fire and Materials 2011 Conference, Interscience Communications, London*, pages 479–492, 2011.

[37] Kathy Murphy, Tim Rich, and Tim Sexton. An assessment of fuel treatment effects on fire behavior, suppression effectiveness, and structure ignition on the angora fire. 2007.

[38] Sean Rissel and Karen Ridenour. Ember production during the bastrop complex fire. *Fire management today*, 72(4):7–13, 2013.

[39] Mohamad El Houssami, Eric Mueller, Alexander Filkov, Jan C Thomas, Nicholas Skowronski, Michael R Gallagher, Kenneth Clark, Robert Kremens, and Albert Simeoni. Experimental procedures characterising firebrand generation in wildland fires. *Fire Technology*, 52(3):731–751, 2016.

[40] Ali Tohidi, Nigel Kaye, and William Bridges. Statistical description of firebrand size and shape distribution from coniferous trees for use in metropolis monte carlo simulations of firebrand flight distance. *Fire Safety Journal*, 77:21–35, 2015.

[41] SR Tursns. *An introduction to combustion, concepts and applications*. McGraw-Hill, New York City, 2012.

[42] T Kehoe, J Bryner, V Reboud, J Dual, and CM Sotomayor Torres. Nano-scale effects on young's modulus of nanoimprint polymers measured by photoacoustic metrology. In *Journal of Physics: Conference Series*, volume 214, page 012049. IOP Publishing, 2010.

[43] Stéphane Cuenot, Christian Frétigny, Sophie Demoustier-Champagne, and Bernard Nysten. Surface tension effect on the mechanical properties of nanomaterials measured by atomic force microscopy. *Physical Review B*, 69(16):165410, 2004.

[44] E Virot, A Ponomarenko, É Dehandschoewercker, D Quéré, and C Clanet. Critical wind speed at which trees break. *Physical Review E*, 93(2):023001, 2016.